UNIVERSITY OF PADOVA

FACULTY OF ENGINEERING

DEPARTMENT OF ELECTRONICS ENGINEERING

Master Thesis

The stochastic neural network in VLSI for studying noise communication in crayfish

Thesis Advisor

Prof. Andrea Gerosa

Candidate

Agostino Benvegnú

Academic Year 2012–2013

Contents

Introduzione **4**

1 From Biology to Neuron Model **13**

1.1 The neuron 13

1.2 The action potential 16

1.3 The synapse 17

1.4 The neuronal dynamic 19

1.5 The Hodgkin-Huxley formalism 20

1.6 The simplified HH model 22

1.7 The neural families 23

1.8 Synapse model 25

2 Stochastic Neuron Model **27**

2.1 Noise 27

2.2 An introduction to stochastic differential equations 28

2.2.1 Probability space 28

2.2.2 Random variable and random process 29

2.2.3 Brownian motion 30

2.3 Stochastic differential equations 31

2.4 Methods for incorporating noise in HH models 33

2.5 Results of stochastic model 34

3 Modeling of CPR Network **39**

3.1 Biology CPR Network 39

3.2 CPR network model 42

3.2.1 CPR neuron 45

3.2.2 The HN and IN neurons 47
3.2.3 The synapse in the CPR network 48

4 Design CPR Network **53**
4.1 Design principle of conductance based model 53
4.2 From biology to hardware implementation 55
4.3 Elementary circuits for neural analog functions 56
4.3.1 Voltage-current converter 57
4.3.2 Current-mode multiplier 57
4.3.3 Operational transconductance amplifier 59
4.3.4 Bipolar differential pair with predistortion stage 61
4.4 Library of neural analog operator 63
4.4.1 Sigmoid function 63
4.4.2 Kinetic function 64
4.4.3 Power raising 65
4.4.4 Output multiplier 66

5 Noise Implementation **69**
5.1 Noise generator 69
5.1.1 Sigma-delta modulation 69
5.1.2 Cellular structure 71
5.2 Noise generator implementation 73
5.2.1 Switched capacitor integrator 73
5.2.2 Behaviour of sigma-delta modulation 75
5.2.3 CMOS implementation 78
5.3 Results 85
5.4 Noise implementation into gating variables 87

6 Conclusion **91**
6.1 Future work 92

To my family

"Stay Hungry. Stay Foolish."

-Steve Jobs-

Sommario

L'attività neurale in natura presenta un andamento stocastico e gioca un ruolo significativo nel cervello. Tuttavia, la maggior parte degli articoli si limitano alla simulazione di neuroni stocastici. In questa tesi, proponiamo un nuovo modello stocastico secondo il formalismo di Hodgkin-Huxley basato su equazioni differenziali stocastiche e moto browniano. Il nuovo modello di equazione differenziale stocastiche riproduce una vasta gamma di dinamiche in modo più realistico rispetto ai precedenti modelli deterministici. Tale modello stocastico è stato applicata a una semplice rete neurale che si trova sulla coda di un gambero chiamato CPR (caudal photoreceptor). Presentiamo una libreria di operatori analogici stocastici utilizzati per il calcolo analogico in tempo reale. Questa libreria permette di ottenere una implementazione in silicio della rete stocastica CPR che sarà collegata alle cellule nervose del gambero. L'interazione vivente-artificiali permetterà ai biologisti di comprendere meglio i fenomeni nervosi.

Abstract

The Neural activity in nature presents a stochastic trend and plays an important role in the brain. However, most papers are limited simulating stochastic neurons. In this thesis, we propose a novel stochastic model according to the Hodgkin–Huxley formalism using stochastic differential equations and Brownian motion. The new stochastic differential equation model reproduces a large range of dynamics more realistically than previous deterministic models. Such stochastic model has been applied to simple neural network that is located on the tail of the crayfish called CPR (caudal photoreceptor). We present

a library of stochastic analog operators used for the analog real-time computation. This library allows to obtain a silicon implementation of the CPR stochastic network that will be connected to the nerve cells of the crayfish. The living-artificial interaction will allow biologists to better understand the nervous phenomena.

Introduction

This thesis is part of a wider research on the effects of noise in the nervous system, which is one of the most interesting topics in neuroscience. In the last decade, biologists and engineers have sought to study complex systems of neural networks, like the nervous system, through the observation and the analysis of the electro-physiological phenomena. There are networks which are too complex to analyse, so we reduce to consider smaller networks with the same electrophysiological phenomena. This helps us to understand the possible mechanism of signal processing.

In our case, we are going to add noise to a small network to study the stochastic behaviour of this network. We will analyse a particular network of interest for the study of noise for biologists, which is located in the tail of the crayfish and is called CPR (caudal photoreceptor). In this network, there are two types of neurons that are sensible to the stimuli of light and mechanical forces. When they are stimulated, they generate a neural command and act as a switch that turns on the corresponding locomotion network to produce a movement. In order to study the communication between the neurons of the crayfish, we have reproduced a network with six neurons and twelve synapses according to the model proposed in the Hodgkin-Huxley formalism.

This thesis work has been made in collaboration with the National Tsing Hua University in Taiwan and it proposes the hardware implementation of an artificial neural network that will be connected to the nerve cells of the crayfish. The realisation of this network will allow biologists to understand the mechanisms of biological living cells and the effects of the noise in biological neurons.

Recently, thanks to its continuous development and improvement, the Very Large

Scale Integration (VLSI) technology has been largely applied to communication and other computational systems since it allows to integrate multiple and complex functions in the custom integrated circuits (ICs). The efficiency, low power dissipation and high integration level of CMOS VLSI technology make it an excellent candidate to realise our device. The combination of the VLSI with the biological structure allows us to build a bio-hybrid system and to take advantage of both. The study of neural communication will be based on the interaction between the artificial, mathematically modelled neurons of hybrid biochips and living neurons. The biological neurons are from five to six times slower than conventional electronic components: an event in a chip occurs in some nanoseconds (10^{-9} s) while a neural event in a few milliseconds (10^{-3} s). So, it becomes necessary to design a real-time chip and operate under the same biological frequencies. One of the major difficulties in the implementation is the need to solve a real-time equations that makes up the artificial part. The path we have chosen for the realisation of this task is the design and use of analogue circuits. This choice implies a costly design (silicon area, number of pads, power consumption), but it is an interesting alternative to digital computation in simulation platforms due to its locally analog and parallel nature of the computations.

This thesis moves on the axis of research of **Architecture of Silicon Neural Networks** team at IMS Laboratory of Bordeaux, which designs and develops integrated circuits for analog and digital neural architecture. The realisation of the stochastic neural network will rely on the previous work of the team, including a library of analog mathematical operators, according to the Hodgkin-Huxley formalism.

In recent times, engineers, biologists and mathematicians have reached a deeper knowledge of stochastic neurons, but no one realized until now the neuron ICs to test these discoveries. To meet these requirements, we propose in this thesis to study and model the noise in the gating variable and consequently we present a new stochastic Hodgkin-Huxley model, which can reproduce a wide dynamic range, more realistic than previous deterministic models. From this stochastic model we have designed the IC, that is optimized for reproducing the CPR network thanks to tunable parameters.
The objectives of the project can be summarized as follows:

1. Synapse Modeling;

2. Stochastic neuron modeling;

3. CPR network modeling;

4. Design a configurable, scalable and stochastic VLSI of CPR network.

Our work is divided in 5 chapters that we briefly summarize below.

The first chapter of the thesis will be devoted to a brief introduction to simple concepts of neurophysiology; in particular, we report a schematic description of neurons and synapses. We will describe the phenomenology of neuronal dynamics, especially the generation of the action potential in terms of the dynamics of the ionic currents that pass through the neuronal membrane. Finally, we will discuss the Hodgkin-Huxley model that we have decided to implement on silicon and its simplified model.

The second chapter will be devoted mainly to the stochastic neuron. We will give a brief introduction on the basic mathematical concepts used to solve a precise stochastic differential equation. After that we will model the stochastic noise of a neuron and find out what are the possible configurations of the equations describing the Hodgkin-Huxley model. Finally, we will show the simulation results of the chosen implementation.

In the third chapter, we will describe the CPR network and its electro-physiological phenomena, namely the different types of neurons and synapses that built it. Finally, we will show all the Matlab simulations of the network.

In the fourth chapter, we will discuss the pioneering work of design of integrated circuits neural, in particular the model that we will chose to implement in silicon. We will define in details all the different mathematical operators and their building blocks.

In the fifth chapter, we will describe the implementation of the noise generator, in particular we will analyse the operation of a single cell and the operation of sixty-four cells in cascade. We will also propose the Hardware implementation of noise into gating variable.

In conclusion, we will report the main results obtained in this thesis along the prospects and the possible future applications of these studies.

Chapter 1

From Biology to Neuron Model

In this chapter we introduce the basic knowledge need to understand the biological model of neurons that we should deploy across the silicon circuit. In the first part of the chapter, we describe the physiology of the neuron and synapse; we analyse the electrical activity emitted during the dynamic phase of the neuron. At the end of the chapter, we define the mathematical model, that describes the behaviour of biological neuron, and that it is implemented in our chip.

1.1 The neuron

The neuron is an electrically excitable cell dedicated to the transfer, storage and processing of information through electrical and chemical signals. Neurons are basic units of neural

Figure 1.1: Cortex neurons of mammals observed by microscope. We can distinguish neurons with triangular and circular cell bodies: cell b is a classic example of a pyramidal cell with a triangular body [1]

network, as the brain. Each neuron has a specialized task: e.g. sensory neurons respond to touch, sound, light but no other stimulation. The number of neurons in the brain is very large, about 100 billion according to recent estimates. The neurons are connected with one another in really complex networks. In Figure 1.1 is shown schematically a small

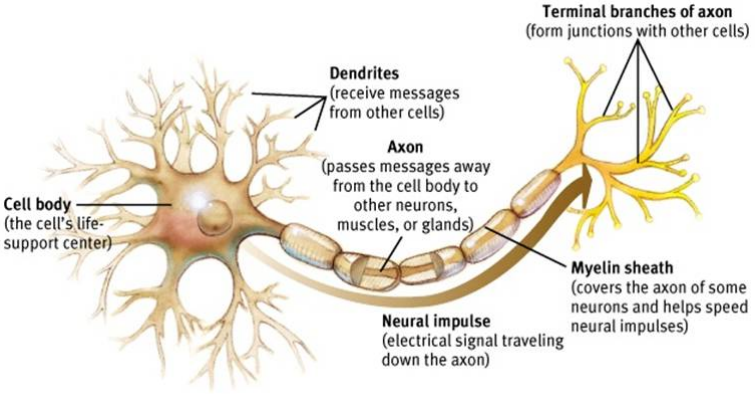

Figure 1.2: Structure of a typical neuron [2].

part of a network of neurons.

The neuron is composed of three main parts: soma (or cell body), dendrite and axon (as Figure 1.2).

The **soma**, that is the central part of the neuron, contains the nucleus of the cell. Its shape is variable according to the type of neuron: it can be pyramid-shaped, oval or spherical (of about $20\mu m$ of diameter in the human cortex) and is essentially the information processing unit.

The **dendrites** are highly branched extensions of the soma, their extension can reach millimeters. They allow synaptic connections and their function is to collect signals coming from other neurons and transmit them to the soma.

The **axon** is a long protuberance which can extend for tens, hundreds or even tens of thousands times the diameter of the soma in length. They are projected from the soma itself. Its function is the transmission of the signal generated from the cell body toward the dendrites of another neuron. The terminal portion of the axon comes into contact with dendrites or soma of other cells, forming a particular structure, called "synapse".

If you think the neuron as an electronic device, it is possible to say that the dendrites are the input terminals ("input"), the soma is the unit of information processing, and the axons are the output terminal ("output").

Around the just described structure, we find the cell membrane of the neuron which is

composed of lipids and proteins. It serves as barrier between intracellular and extracellular environment and is composed of a lipid bilayer (as in Figure 1.3). In this lipid barrier there are several protein molecules that pass through the entire thickness of the cell membrane, bringing into contact the intracellular and extracellular environment. These particular proteins are called protein channels, channels or membrane ion channels. They allow the transport of every kind of molecules. Without them the cell membrane can be penetrated by substances from outside to inside and vice versa through different mechanisms, but the penetration depends on the degree of solubility in lipids. The inorganic ions, sodium, potassium, calcium and chlorine, that pass through the membrane are the ionic currents at the heart of the electrical activity of neurons. When the membrane is not subject to

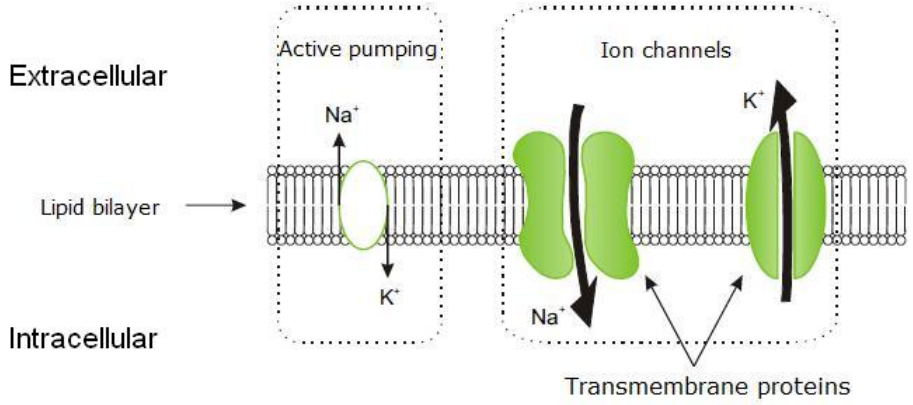

Figure 1.3: Illustration of the lipid bilayer.

any excitation, the system is at rest, the concentration gradient and the electrical one are balanced. The value of the membrane potential which has no neat flow of any ionic species is defined as equilibrium potential of an ionic species. The equilibrium potential of each ionic species is linked to the intracellular and extracellular concentrations, through the Nerst's equation:

$$E_{ion} = \frac{KT}{q} \ln \frac{[n]_e}{[n]_i} \tag{1.1}$$

where E_{ion} is the equilibrium potential of the ion, $[n]_e$ and $[n]_i$ are respectively the extracellular and intracellular concentration; $K \sim 1,38 \cdot 10^{-23}$ J/K is the constant Boltzmann; T is the absolute temperature in Kelvin; and q is the electric charge of the ionic species (in Coulomb). Hence E_{ion} is usually of the order of -65 mV.

1.2 The action potential

Ion channels of the cell membrane are permeable to a single ion species. These channels are voltage dependant; this means that their permeability is linked to the potential difference between the intracellular and extracellular environment. The permeability of these proteins selectively gives rise to the action potential, i.e. an electrical phenomenon which propagates along the axon. The membrane potential is defined as the potential difference measured at the terminals by two electrodes, one set inside the neuronal cell and the other set in the surrounding extracellular fluid. The temporal variation of the action potential develops a neural signal.

The generation of action potentials takes place in 3 main phases, to describe them we will refer to Figure 1.4:

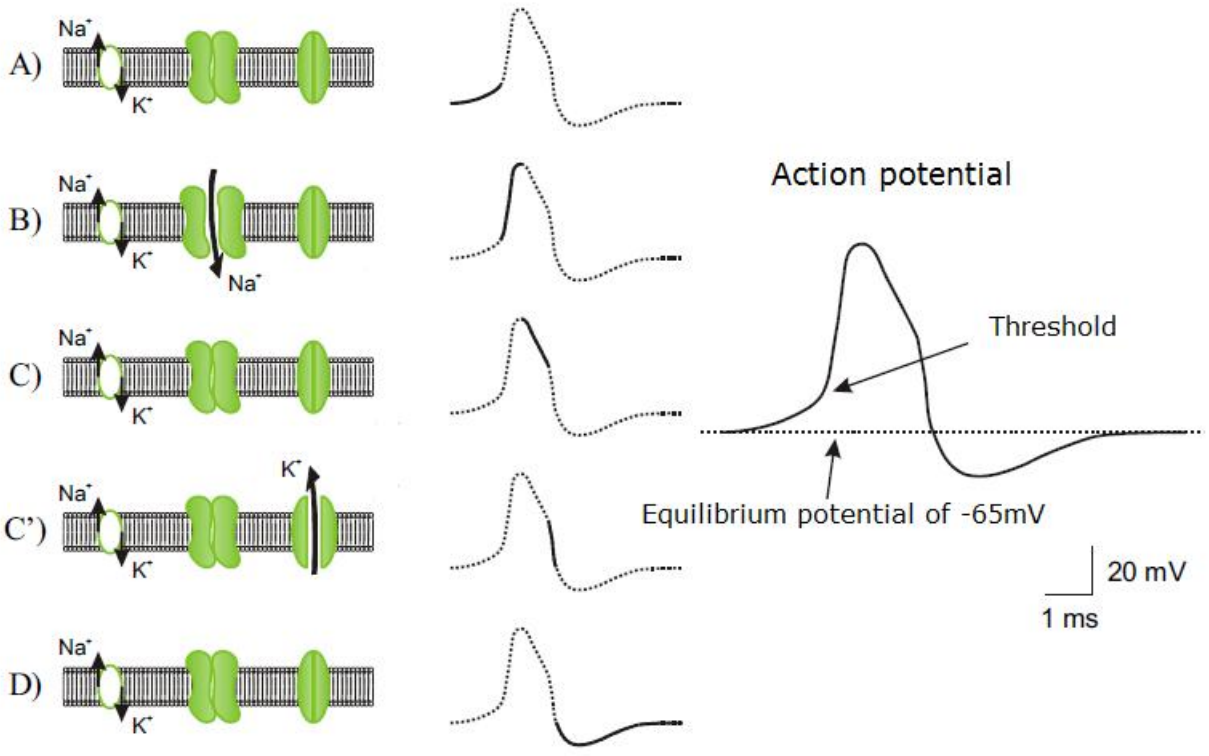

Figure 1.4: The mechanism of origin of the action potential.

1. **Ascending phase** (depolarization). The membrane is in its resting state at a negative potential, around -65mV due to differences in ionic concentrations at the end of an activity cycle. When stimulation induces membrane depolarization it

triggers the rapid opening of the Na^+ channels 1.4 (A). The entry of Na^+ ions, in order to depolarize the membrane, continues even after the arrest of stimulation that only served to exceed the threshold, forcing the membrane from its equilibrium state 1.4 (B).

2. **Descending phase** (repolarization). There are two factors involved in the repolarization of the membrane, the first one is the spontaneous closure, called the inactivation of sodium channels and the second one is the delayed opening of K^+ channels. The dependence of the membrane potential induced by the value reached for the block of the channel sodium makes the action potential decrease 1.4 (C). On the other hand, thanks to the potential flow rates, the opening of potassium channels with a certain delay time induces a K^+ current which accelerates the phenomenon 1.4 (C').

3. **Transient hyperpolarization phase**. The delay in the change of state of the potassium channels is reflected in their closing and causes hyperpolarization of the membrane. At the complete closure of these channels there will result a return to the initial value 1.4 (D). Moreover, for the duration of this phase, that is called Refraetory period, the action potential can not change because the neuron is "insensitive" to stimuli that arrive from the neuron.

1.3 The synapse

The passage of information among neurons in the nervous system occurs through synapses. Each synapse is composed by two different neurons and the surrounding area, this set is called the synaptic cleft. It defines two types of neurons: the presynaptic one (upstream of the synapse) which transmits the action potentials to the next neuron, and the postsynaptic one (downstream of the synapse) which receives the action potentials from the previous neuron.

The synapse is the region where the axon of a presynaptic neuron comes into contact with the dendrite (or soma) of a postsynaptic cell. It also defines the postsynaptic potential voltage response of the postsynaptic neuron, consequent upon the arrival of the action potential from the presynaptic neuron. We distinguish two main types of synapses: electrical synapses and chemical ones.

The **electrical synapses** realize an electrical coupling between two neurons through ion

channels that connect the highly specialized presynaptic membrane and the postsynaptic one. The electrical synapses thus allow a direct current flow between adjacent neurons.

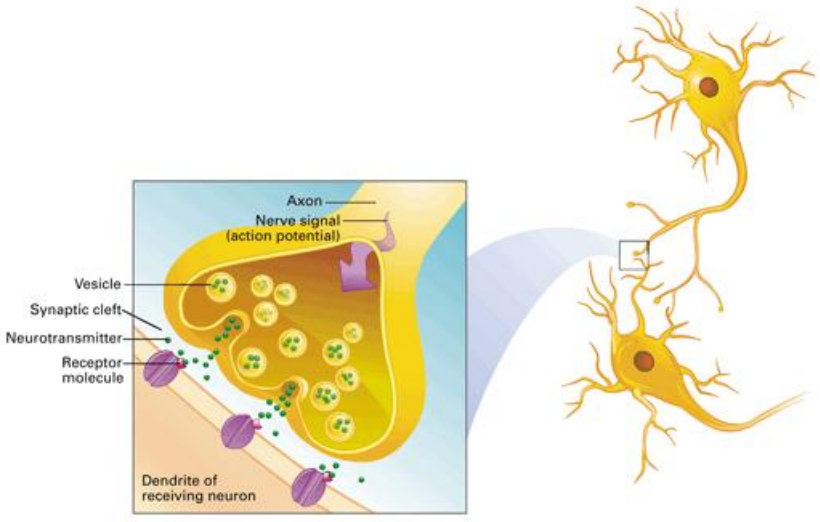

Figure 1.5: Chemical synapse [3].

The **chemical synapse** (Figure 1.5), the most common in the vertebrate brain, is based on the following mechanism: the action potential generated by the presynaptic neuron achieves the end of the axon and locally depolarizes the cell membrane. This is possible thanks to particular structures located into the axon, called synaptic vesicles, which, under the action of membrane potential, release into the synaptic cleft special chemicals called neurotransmitters. As soon as they have reached the postsynaptic side of the synapse, the neurotransmitters compose with chemoreceptors placed on the postsynaptic membrane, causing the opening of specific channels through which a ion current flows from the extracellular fluid to the cell. The entry of these ions in its turn, leads to a variation of the value of the postsynaptic membrane potential. In short in a chemical synapse first occurs the transformation of an electrical signal into a chemical one (on the presynaptic membrane) and then the subsequent transformation on the postsynaptic membrane of a chemical signal into an electrical one.

As we have seen, during the communication between neurons they release neurotransmitters that bind chemicals receptors. A neurotransmitter can be thought as a key, and a receptor as a lock: the same type of key can here be used to open different types of locks. The receptors can be classified generally as excitatory (causing an increase in firing rate), inhibitory (causing a decrease in firing rate) or modulating (causing long lasting effects, not

directly related to the frequency of activation). We cite few examples of neurotransmitters:

- excitatory: glutamate (whose recepters are AMPA / kainate);
- inhibitory: GABA and glycine.

The effectiveness of a synapse is strongly involved in the way in which the network processes the information. The nervous system has the capacity of modifying this operating efficiency in connections between neurons, of creating new links and deleting some others. This property allows the nervous system to change its functionality and its structure in a more or less permanent way, in dependence of the events that affect it, such as, for example, experience and memory.

1.4 The neuronal dynamic

We have already mentioned that the arrival of an action potential at the presynaptic neuron causes a change in the membrane potential of the receiving neuron (postsynaptic potential). This can happen in two ways: excitatory postsynaptic potential and inhibitory postsynaptic potential, according to whether the effect is either to increase or to decrease the value of the membrane potential.
These mechanisms vary according to the type of neuron: for example, the neurons of the cerebral cortex (cortical neurons) have thousands of synaptic contacts (from 10^3 to 10^4) with other neurons in the cortex of which about 85% are excitatory and the rest inhibitory. The role of synapses is crucial for the functioning of the neural system. To understand the mechanism of the synapse, we analyze the dynamic neural activity according to the variation of postsynaptic potential. The postsynaptic potential can be recorded with an intracellular electrode which measures the potential difference $V_M(t)$ between the interior of the cell and its surroundings. The neural dynamic that is established in response to the arrival of pulses from presynaptic neurons is described by the following steps:

- Figure 1.6 A: postsynaptic neuron receives impulses from the two presynaptic neurons j = 1,2; $V_{M_i}(t)$ and $V_{Mrest}(t)$ represent respectively the membrane potential and the value of the resting potential of the neuron i, and the quantity $\epsilon(t - t_1^{(f)})$ corresponds to the postsynaptic potential generated by the arrival time $t_1^{(f)}$ of a pulse from neuron j = 1.

- Figure 1.6 B: a pulse coming from the other presynaptic neuron j = 2 at an instant $t_2^{(f)}$, within a sufficiently short time interval. It causes a second postsynaptic potential which is added to the previous one. In this regime, the response of the postsynaptic neuron is approximately linear in the sense that the answer is approximately proportional to the input that it receives.

- Figure 1.6 C: when $V_{M_i}(t)$ reaches a typical value, θ, called the activation threshold, the behaviour of the neuron becomes highly non-linear: it can generate an action potential that has a stereotyped form and therefore it has no link with the stimuli that has produced it.

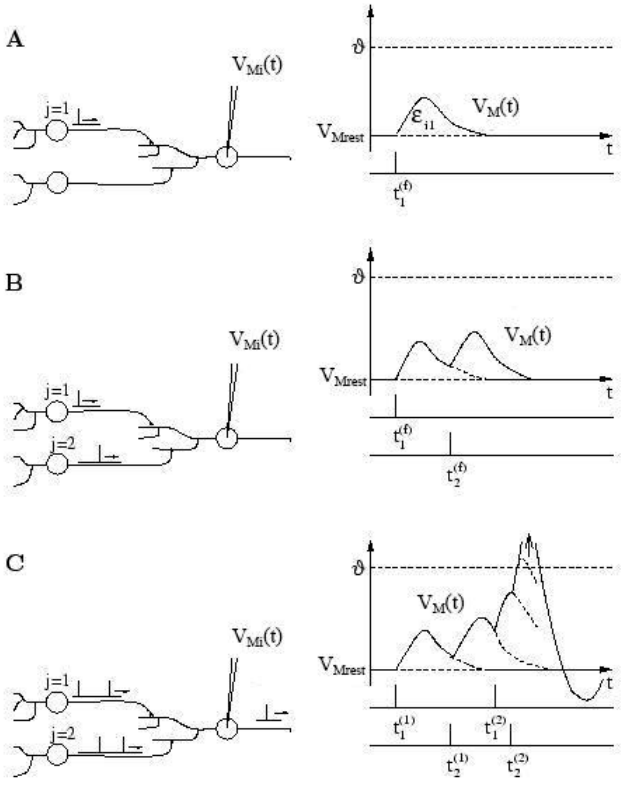

Figure 1.6: Possible evolution of the voltage postsynaptic [1].

1.5 The Hodgkin-Huxley formalism

In 1952 Alan Lloyd Hodgkin and Andrew Huxley described a model which explains the ionic mechanisms underlying the initiation and propagation of action potentials in the squid giant axon. In 1963 they were awarded with the Nobel Prize in Medicine for this

work.

We used the Hodgkin-Huxley formalism as a design for our IC. The main advantage of

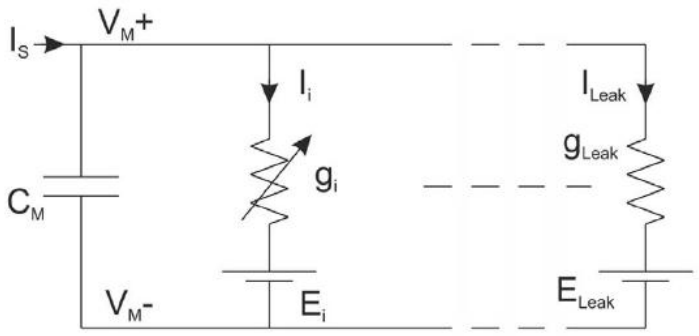

Figure 1.7: Equivalent electrical circuit of a neuron.

this formalism is that it relies on biophysically realistic parameters and it describes individual ionic and synaptic conductances for each neuron in accordance with the dynamics of ionic channels. As mentioned in the previous section, the electrical activity of a neuron is the consequence of the diffusion of different ionic species through its membrane. This behaviour is described by the mathematical model of Hodgkin-Huxley (to which we refer using the abbreviation HH). The HH formalism provides a set of equations and an equivalent electrical circuit(Figure 1.7).

The time derivative of the potential across the membrane is proportional to the sum of the currents, according to the following expression:

$$C_M \frac{dV_M}{dt} = -\sum_I I_i - I_{Leak} + I_S \tag{1.2}$$

where V_M is the membrane potential, C_M is the membrane capacitance, I_i denotes the individual ionic currents of the model, I_{Leak} the leakage current, I_S is a stimulation or a synaptic current. I_i is the current for a given type of channel and its associated equation is:

$$I_i = g_i \cdot m^p \cdot h^q \cdot (V_M - E_i) \tag{1.3}$$

where g_i is the maximum conductance; m and h are gating variables, respectively, for activation and inactivation representing the fraction of available open gates at any given time and voltage. E_i is the ion-specific reversal potential and p and q are integers. With

the simplification of the HH model described in the next section we find m by solving the differential equations 1.4, where τ_m is the time constant for convergence. It depends on the membrane voltage and on m_∞, which is a sigmoid function of V_M (equation (1.5)). $V_{Offset,m}$ and $V_{Slope,m}$ are the offset and the slope of the activation sigmoid. The inactivation parameter h follows identical equations, except for the sign inside the brackets, which is positive.

$$\tau(V_M)\frac{dm}{dt} = m_\infty - m \tag{1.4}$$

$$m_\infty = \frac{1}{1 + exp\left(-\frac{V_M - V_{Offset,m}}{V_{Slope,m}}\right)} \tag{1.5}$$

The original equations proposed by HH model describe sodium, potassium and leakage channels, with $p = 3$ and $q = 1$, $p = 4$ and $q = 0$, $p = 0$ and $q = 0$ respectively, in equation 1.3.

1.6 The simplified HH model

In the original equation of HH model the gating variables are described by the following equation:

$$\frac{dX}{dt} = \alpha_X(V_M)(1 - X) - \beta_X(V_M)X \tag{1.6}$$

where $\alpha_X(V_M)$ and $\beta_X(V_M)$ are functions deduced by empirical datas. We implemented in our chip the HH model with an approximation, that is essentially based on the use of the fixed time constant in equation (1.4). We chose this approximation in order to reduce the number of equations implemented in the chip. If we collect the variable X to the right of the equation (1.6) we obtain the following expression:

$$X = \frac{\alpha}{\alpha + \beta} - \frac{1}{\alpha + \beta}\frac{dX}{dt} \tag{1.7}$$

Then to rewrite the equation (1.6) in the form (1.4), we must follow the three steps:

1. Compute $\alpha_X(V_M)$ and $\beta_X(V_M)$ from biological patterns over the range V_M =[-80, +50]mV.

2. Identify $V_{Offset,x}$ and $V_{Slope,x}$ in terms of the sigmoid function that is equal to $X_\infty = \frac{\alpha_X(V_M)}{(\alpha_X(V_M)+\beta_X(V_M)}$.

3. τ_x compute from $\tau_x = \frac{1}{(\alpha_X(V_M)+\beta_X(V_M))}$. The value of V_M is chosen empirically and $-70mV$ is the best value.

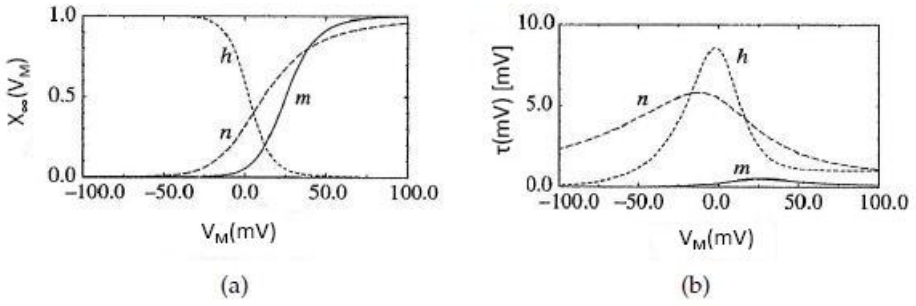

Figure 1.8: .Equilibrium function (a) and time constant (b) for the variables m,n,h in the HH model. The resting potential is at V_m=0.

The trends of gating variable of the original HH model are shown in Figure 1.8.

1.7 The neural families

The HH formalism is much more complex and precise than simple models. It allows us to emulate different types of neurons. The types of neurons that have been implemented so far [4] with this formalism are the following: FS (Fast Spiking), RS (Regulan Spiking), IB(Intrinsically Bursting) and LTS (Low-Threshold Spiking). Table 1.1 summarizes the conductances that compose the FS, RS, IB and LTS neurons.

Neuron's types	**Conductances**
FS	$I_{Leak}(p=0,q=0), I_K(p=3,q=1), I_{Na}(p=4,q=0)$
RS	$I_{Leak}(p=0,q=0), I_K(p=3,q=1), I_{Na}(p=4,q=0), I_{Slow,K}(p=1,q=0)$
IB	$I_{Leak}(p=0,q=0), I_K(p=3,q=1), I_{Na}(p=4,q=0), I_{Ca,L}(p=2,q=1)$
LTS	$I_{Leak}(p=0,q=0), I_K(p=3,q=1), I_{Na}(p=4,q=0), I_{Ca,M}(p=2,q=1)$

Table 1.1: Extracted of the conductances of FS, RS, IB and LTS neurons.

This division corresponds to classify cells [5] according to presence or absence of the three following criteria:

- spike-frequency adaptation;
- burst discharges from depolarizing stimuli;
- burst (or any other type of) discharge following hyperpolarizing inputs (rebound response).

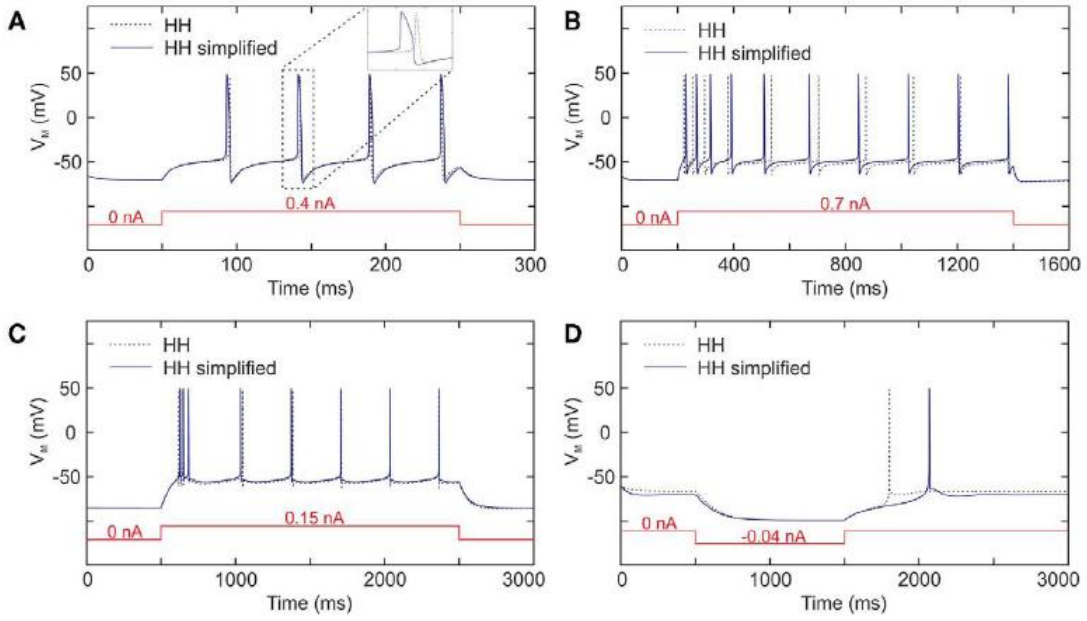

Figure 1.9: Membrane voltage software simulation of HH model for (A) FS neuron, (B) RS neuron, (C) IB neuron and (D) LTS neuron [4] .

.

The first model is FS neuron. This cell is the simplest model; it is formed by the conductances for generating spikes (I_{Na}, I_K, I_{Leak}). The FS neurons correspond to inhibitory neurons and respond to depolarizing pulses by producing high frequency trains of action potentials without adaptation. Thus their frequency is constant during the stimulation (Figure 1.9 A).

Another common cell class in neocortex is called the RS neuron, which is, in general, excitatory and most often corresponds to spiny pyramidal-cell morphology. The typical responses of RS cells to depolarizing current pulses are trains of spikes with adaptation; in detail we observe a high frequency discharge on the first part of the response and then the frequency decreases slowly due to the adaptation phenomenon (Figure 1.9 B). The RS model adds slow potassium current activated ($p = 1$ and $q = 0$) by depolarization, more than the FS model.

Another cell class is the IB neuron, that is represented by a few percent of the recorded cells in primary sensory cortex. This kind of neuron generates bursts of action potentials following depolarizing stimuli and then the firing rate decreases immediately. To generate the bursting behaviour, we extend the previous model of RS cell adding the L-type calcium current. Even though the membrane voltages are comparable for the switching frequencies

behaviour, the effect of the L-type calcium current ($p = 2$ and $q = 1$) is to suddenly bring the neuron from one spiking frequency to another (Figure 1.9 C).
The last cell class is LTS, whose activities are described in a significant fraction of intracellularly cells records in animal association cortex and the recordings obtained from the LTS neuron are rare. These LTS neurons generate adapting trains of action potentials in response to depolarizing current injection, similar to the classic "regular spiking" response of cortical neurons. In addition, they generate a burst of action potentials in response to injection of hyperpolarizing current pulses (Figure 1.9 D). We extended the previous model of the RS cell by adding the T-type (low-threshold) calcium current, its trend is similar to IB spiking.

1.8 Synapse model

So far we have described only about the neuron model, but to realize our mini artificial neural network we need to define a model for the synapse. As we have seen at the biological level, electrical synapses are created by pairs of twisted junction channels, allowing a flow between the intracellular environments of the two neurons entering into very fast communications. The conductance of these channels is generally symmetrical and independent of the voltage membrane. Therefore, they are modeled by a simple conductance and they are called ohmic synapses. Recalling the description of electrical synapses and the transmission of neural action potentials, we underline that in this case it is considered better an approach based on the network that does not take into account these electrical synapses.
Modeling chemical synapses is generally based on the pattern established for the voltage-dependent ion conductances. Reminding what discussed earlier on the operating mechanism of chemical synapses, we have considered the ion current induced in the postsynaptic cell by neurotransmitters transmitted by the presynaptic neuron; in particular we looked at the dependence of the activation function in relation to the presynaptic membrane voltage and secondly at a weighting of the same current on the postsynaptic membrane. In other words, we can formulate these dependencies of the three following mathematical expressions:

$$I_{Syn} = g_{Syn} \cdot r(V_{M_{pre}}) \cdot (V_{M_{post}} - E_{Syn}) \tag{1.8}$$

$$\tau \frac{dr}{dt} = r_{\infty}(V_{M_{pre}}) - r \tag{1.9}$$

$$r_{\infty}(V_{M_{pre}}) = \frac{1}{1 + exp\left(-\frac{V_{M_{pre}} - V_{Offset,m}}{V_{Slope,m}}\right)} \tag{1.10}$$

Where g_{Syn} is the maximum conductance of the synapses and E_{Syn} is the equilibrium potential of the electrochemical ion species. In equation 1.8, we consider the synaptic current negative (positive) when it enters (exits) in the post-synaptic cell. Chemical synapses can be excitatory or inhibitory, this property will be determined by the value of E_{Syn}. In the case of an excitatory synapse E_{Syn} will be around 0 mV, in the case in which it is inhibitory of about -100 mV. It is supposed that the voltage membrane of the postsynaptic neuron is at its resting potential, for example, -65 mV, and it is considered the case of observing the influence of inhibitory synapses. When presynaptic action potential will stimulate the synapses, the current calculated using equation (1.8) will be positive. It will lead to hyperpolarization of the post-synaptic cell. Meanwhile, in case of excitatory synapses, the induced current depolarizes the postsynaptic neuron. An important feature of the synapse is the pose that attaches to the post-synaptic signals it receives, that in equation (1.8) is given by the parameter g_{Syn}. The evolution of the synaptic weight will result in a change of the parameterized g_{Syn}. In this study of the phenomena learning or plasticity of the network are not taken into account, infact in our case, g_{Syn} is a constant.

Chapter 2

Stochastic Neuron Model

As we have explained in the introduction, the noise in the key of many events in the brain but its role is almost unknown and this has increased the interest for Neuroscience. In this chapter, we introduce the use of stochastic differential equations (SDE) and Brownian motion in describing the dynamics of multi-conductance Hodgkin-Huxley model, see [6], [7], [8]. Namely we analyse where it is better to add the noise in the HH model and the effects that it produces.

2.1 Noise

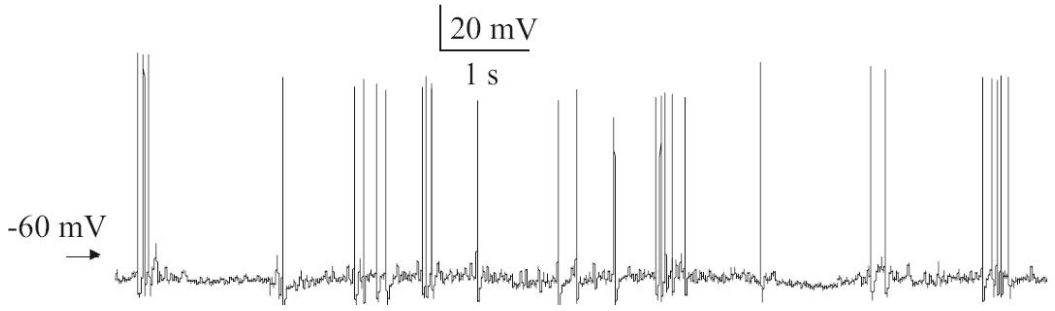

Figure 2.1: In vivo recording of a layer of 5 pyramidal cell in rat prefrontal cortex [9].

The stochasticity is one of the key elements in describing information processing in the brain and may as well play an interesting role in the dynamic behaviour of neurons, see [10], [11]. For example, the stochastic activity can be observed by the following experiment on the visual cortex's neuron: if we move a bar in the visual field of an animal, we can notice that the activation frequency of the visual cortex changes until the bar goes out of the visual field. If you try again the same experiment, the neural activity will vary greatly

because the neurons are affected by the noise. It can also be observed that the neuron has spontaneous activity even if the screen is blank, see [12].
Many in vivo experiments show noisy behaviour of neurons, as we can see in the Figure 2.1. The neural activity in vivo shows a much more irregular behaviour. With the SDE in the HH model we try to model the stochastic behaviour of neurons that takes place in nature. The noise in the brain is generated by intrinsic noise sources that give birth to stochastic behaviour in the neuronal dynamics (properties of single neurons) and extrinsic sources that arise from network effects and synaptic transmission. It depends on the level of activation of neuromodulatory systems and it is correlated with the functional state of the brain.

2.2 An introduction to stochastic differential equations

In this chapter we recall some fundamental notions of probability theory, such as the notions of probability space, random variable, random process and Brownian motion. These concepts allow us to have a minimal background for understanding the resolution of stochastic differential equation.

2.2.1 Probability space

A probabilistic model is a mathematical description of an uncertain situation. Every probabilistic model involves an underlying process, called the experiment, that will produce exactly one out of several possible outcomes. The set of all possible outcomes is called the sample space of the experiment. A subset of the sample space that is a collection of possible outcomes, is called an event. To an event we can associate a positive value between 0 and 1 which represent the likelyhood of the event, 0 will stand for a improbable event, 1 for a certain one. Think about the throw of a dice, we can say that if the dice is balanced the probability of the event "the dice showed 6" is $\frac{1}{6}$. All of these concepts can be rewritten in a more formal way defining the probability space.

Definition 2.1. A **probability space** (Ω, F, P) is a three-tuple, in which the three components are :

1. **Sample space**: A nonempty set Ω called the sample space, which represents all possible outcomes.

2. **Event space**: A collection of F subsets of Ω, called the event space.

3. **Probability function**: A function, $P : F \to [0, 1]$, that assigns probabilities to the events in F. This will sometimes be referred to as a probability distribution over Ω.

The probability function must satisfy several basic axioms:

1. Non-negativity: $P(E) \geq 0$ for all $E \in F$.

2. Normalization: $P(\Omega) = 1$.

3. Countable Additivity: $P(E \cup D) = P(E) + P(D)$ if $E \cap D = 0$, for all $E, D \in F$.

2.2.2 Random variable and random process

In many probabilistic models, the outcomes are numerical, e.g. when they correspond to instrument reading. In other experiments, the outcomes are not numerical, but they may be associated with some numerical interest. This is done through the notion of a random variable.

Definition 2.2. A **random variable** X, in the probability space (Ω, F, P), is a function $X : \Omega \to \mathbb{R}^d$ such that the inverse image

$$X^{-1}(A) = \{\omega \in \Omega : X(\omega) \in A\} \text{ is in F}$$

for all open subsets A of $\mathbb{R}^d$.

In practice, the random variable (function), $p_x = f(E_x)$ is the function that associates to each event partition a real number (probability of event). Random variables can be classified as either discrete (i.e. they may assume any of a specified list of exact values) or as continuous (i.e. they may assume any numerical value in an interval or collection of intervals). The mathematical function describing the possible values of a random variable and their associated probabilities is known as a probability distribution.

There are several basic concepts related to random variables, which are summarized in the following points:

- A random variable is a real-valued function of the outcome of the experiment.

- A function of a random variable defines another random variable.

- We can associate with each random variable certain "average" of interest, such as the mean and the variance.
- A random variable can be conditioned of independent on an event or on another random variable.

In probability theory, a stochastic process is a collection of random variables. It is often used to represent the evolution of some random value, or system, over time. Instead of describing a process which can only evolve in one way (as in the case, for example, of solutions of an ordinary differential equation), in a stochastic or random process there is some indeterminacy: even if the initial condition (or starting point) is known, there are several (often infinitely many) directions in which the process may evolve.

Definition 2.3. A **stochastic process X** with state space S is a family $X = \{X_n\}_{n\in I}$ or $\{X_n : n \in I\}$ of random variables $X_i : \Omega \to S$, where I is an index set, defined on a common probability space (Ω, F, P).

2.2.3 Brownian motion

The Brownian motion is a mathematical model used to describe random movements in atoms or molecules. The Brownian motion, see [13], called also the standard Wiener process, is one of the most import stochastic process in continuous-time.

Definition 2.4. A stochastic process $\{W_t\}_{t\geq 0}$ is called a **standard Wiener process** if it satisfies the following three conditions:

1. $W_0 = 0$;
2. $\{W_t\}_{t\geq 0}$ has independent , i.e. W_{t_1}, $W_{t_2} - W_{t_1}$, ..., $W_{t_k} - W_{t_{k-1}}$ are independent random variables for all $0 \leq t_1 < t_2 < t_3 < \cdots < t_k < \ldots$;
3. for $0 \leq s < t$ the random variable given by the increment $W_t - W_s \sim N(0, t-s)$ where $N(u, \sigma^2)$ denotes the normal gaussian distribution with expected value μ and variance σ^2.

The Wiener process is a Gaussian process: a stochastic process X is called a Gaussian process if for any instant $t_1, ..., t_k$ the vector of random variables $(X_{t_1}, ..., X_{t_k})$ follows a k-dimensional normal distribution. The Wiener process is continuous with zero mean and variance proportional to the elapsed time: $E(W_t) = 0$ and $Var(W_t) = t - s$.

2.3 Stochastic differential equations

A one-dimensional dynamical system is described by the ordinary differential equation

$$\frac{dx}{dt} = g(x,t) \tag{2.1}$$

where it is assumed that $g(\cdot)$ fulfills conditions such that an unique solution exists, $x(t) = x(t, x_0, t_0)$ is a solution satisfying the initial condition $x(t_0) = x_0$. Given the initial condition, we know how the system behaves at all times t, even if we cannot analytically find a solution. These differential equations do not suffice to correctly and realistically model all biological systems, thus we need to allow for some randomness in the description. An ordinary differential equation, to which a noise term is added, is called a stochastic differential equation.

Definition 2.5. The **stochastic differential equation** is a differential equation in which one or more of the terms of the mathematical equation are stochastic processes.

A standard example of stochastic differential equation is a an Ito's equation for a diffusion process. It can be written as

$$dX_t = \mu(t, X_t)dt + \sigma(t, X_t)dW_t \tag{2.2}$$

where X_t is a stochastic process, W_t is a Wiener process, $\mu(\cdot)$ and $\sigma(\cdot)$ are the functions. To solve such equation on time T we have to integrate, obtaining the following:

$$X(t) = X_{t_0} + \int_{t_0}^{T} \mu(s, X_s)ds + \int_{t_0}^{T} \sigma(s, X_s)dW \tag{2.3}$$

where X_{t_0} is a constant. The first integral can be ordinarily solved, while the second, where we have a stochastic process, is called Ito's integral. In discrete time we can approximate the Ito's integral following the classical approach as:

$$\int_{t_0}^{T} \sigma(s)dW_s = \sum_{j=1}^{n} \sigma(t_j)(W(t_{j+1}) - W(t_j)) \tag{2.4}$$

where $(t_j)_{j\geq 0}$ is a partition of $[t_0, T]$. If $\sigma(s, X_s) = \sigma$ is constant, then the solution of the integral (2.13) is

$$\int_{t_0}^{t} \sigma(s)dW_s = \sum_{j=1}^{n} \sigma(W(t_{j+1}) - W(t_j)) = \sigma(W(t) - W(t_0)) \sim \sigma N(0, t - t_0) \tag{2.5}$$

Now we want prove that in continuous time the Ito's integral is distributed like a normal distribution times, the constant σ.

The integral $\int_{t_0}^{T} \sigma dW_t$, where T is a fixed ending time, σ is a constant and W_t is a Wiener process is not a ordinary integral i.e. it cannot be solved using Riemmann or Lebesgue integration since the paths of W_t, for any t, are not smooth. Hence, in order to solve this integral, we need to use a different theory, which is Ito's integral, see [14]. This integral is defined as a limit in probability of Riemmann sums, since such a limit does not exist pathwise. If $\{\Pi_n\}_{t\geq 0}$ is a sequence of partitions of the interval [0,T] such that the mesh of the position Π_n is given by n intervals from $0 = t_0 < t_1 < \cdots < t_n = T$, then the Ito integral of σ against W_t is a random variable given by:

$$\int_0^T \sigma dW_t = \lim_{n\to\infty} \sum_{[t_{j-1},t_j]\in\pi_n} \sigma(W(t_j) - W(t_{j-1})) \tag{2.6}$$

One can show that this limit is well defined and converges in probability. In particular, define $S_n := \lim_{n\to\infty} \sum_{[t_{j-1},t_j]\in\pi_n} \sigma(W(t_j) - W(t_{j-1}))$. Since for each choice of times t,s with $0 \leq s < t$, we have that $W_t - W_s$ is a distributed as a gaussian $N(0, t-s)$, then also S_n, being the finite sum of gaussian variables(σ is constant), is gaussian. Let us compute the expected value of S_n and the variance. Since $W_t - W_s \sim N(0, t-s)$ for $0 \leq s < t$ then $E(S_n)$=0. To compute the variance we have to calculate:

$$E\left(\sum_{[t_{j-1},t_j]\in\pi_n} \sigma(W(t_j) - W(t_{j-1}))^2\right) = \sum_{i,j=1} E(\sigma(W(t_j) - W(t_{j-1}))\sigma(W(t_i) - W(t_{i-1}))) \tag{2.7}$$

where the equality follows applying properties of the expected value. If $i < j$ then $W(t_j) - W(t_{j-1})$ is independent of $W(t_i) - W(t_{i-1})$ by definition of Wiener process, then $E(\sigma^2(W(t_j) - W(t_{j-1}))(W(t_i) - W(t_{i-1}))) = E(\sigma^2(W(t_j) - W(t_{j-1})))E((W(t_i) - W(t_{i-1}))) = 0$. Hence i=j so the sum in (2.14) is equal to

$$\sum_{j=1}^{n} E(\sigma^2(W(t_j) - W(t_{j-1}))^2)) = \sum_{j=1}^{n} \sigma^2 E((W(t_j) - W(t_{j-1}))^2)) =$$

$$= \sum_{j=1}^{n} \sigma^2(t_j - t_{j-1}) = \int_0^T \sigma^2 dt = \sigma^2 \tag{2.8}$$

where the equality is true in probability. Hence S_n is distributed like a normal gaussian $N(0, \sigma^2) = \sigma N(0, 1)$. For the central limit theorem in probability we have that

$\lim_{n\to\infty} S_n \sim \sigma N(0,1)$. Hence we can conclude that

$$\int_0^T \sigma dW_t \sim \sigma N(0,1) \tag{2.9}$$

In particular, let us remark that this process is a Markov process [15], hence it is with no memory, so we can forget about all data before time T when computing its value at time T+1.

2.4 Methods for incorporating noise in HH models

To model the noise in the channels we use the differential equations of the HH model, seen in the previous chapter. We try to introduce the fluctuations in that model. There are mainly two approaches, look at [16] [17] [18] [19], namely:

- **Current noise** is the simplest method to incorporate noise into the HH equations. It consists in adding noise in the current term into the equation of membrane voltage, as shown in the following:

$$C\frac{dV}{dt} = -g_{Na}m^3h(V - E_{Na}) - g_K n^4(V - E_K) - g_L(V - E_L) + I + \sigma dW \tag{2.10}$$

  where σdW is a Brownian motion. This approach is interesting for its simplicity: the noise is generated by the current, which in turn is induced by membrane voltage and consequently by ion channels activity. Nevertheless, this approach is not precise. It has already been implemented by our research group, and has been included in the noise current external stimulation [20].

- **Gating variable** is the most precise and realistic approach to incorporate the stochasticity into terms of activation and inactivation m, n and h of ionic conductances (gating variables), where each gating variable can be randomly either in an open or closed state of the functions rate of activation or inactivation processes. In HH model the configuration of the ion channel is determined by the states of gating. For example, each sodium channel is composed of four n gating variables, all of which must be either open or closed because the channel is permeable to sodium ions. The degree of opening of the channel is determined by the value of the gating variable which can be between 0 and 1. Moreover, the best place to add noise may be in the equations that describe the channel configuration, describing exactly what

happens in nature. The situation just mentioneted is represented by the following formula:

$$dX = \frac{X_\infty - X}{\tau}dt + \sigma dW \tag{2.11}$$

where $\sigma dW$is the Brownian motion and the gating variables X=m,h, or n. The addition of Brownian motion, in this position, models the effects of random openings and closings of ion channels and the random extrasynaptic inputs ones and contributing to the very delicate subthreshold-membrane dynamics in neurons.

The integral form of the SDE 2.11 is the following:

$$X(t) = X_0 + \int_0^t \frac{X_\infty - X(s)}{\tau}ds + \int_0^t \sigma dW \tag{2.12}$$

The Wiener process $(W_t)_{t\geq 0}$ has independent increments i.e. for $0 \leq s < t$, the random variable $W_t - W_s$ is distributed like a normal gaussian $N(0, t-s)$; so, fixed $\epsilon \geq 0$ small, such that $t-s=\epsilon$, then $W_{s+\epsilon} - W_s$ is distributed like $N(0,\epsilon)$. For infinitesimal increments in time, is then clear that dW_t can Using the Ito's integral in the previous section and this approximation, we can rewrite the SDE as

$$\frac{dX}{dt} = \frac{X_\infty - X}{\tau} + \sigma\xi_t(t) \tag{2.13}$$

2.5 Results of stochastic model

We use this stochastic Hodgkin-Huxley model, that we are able to simulate in MATLAB programming environment, to characterize and model our stochastic neuron. Moreover, during the simulation of the stochastic neuron we have tried to lock in continuous time using Simulink and VerilogA but we did not have similar results because they don't have a stochastic differential equation solver.

From the simulations in Matlab of a stochastic neuron, we have noted that equation (2.13) does not produce the desired characteristics of a neuron stochastic. For these simulations we used the FS neuron model in order to simplify and validate our stochastic model. Then, we introduced a constant factor C_τ in the term of noise that is proportional to the time constant τ. The stochastic differential equation (2.13) becomes

$$\frac{dX}{dt} = \frac{X_\infty - X}{\tau} + C_\tau\sigma\xi_t(t) \tag{2.14}$$

The values of C_τ for the different gating variables the neuron FS are the following: $C_{\tau,m}$=3 for m, $C_{\tau,h}$=50 for h, and $C_{\tau,n}$=20 for n. In the simulations of stochastic model (described

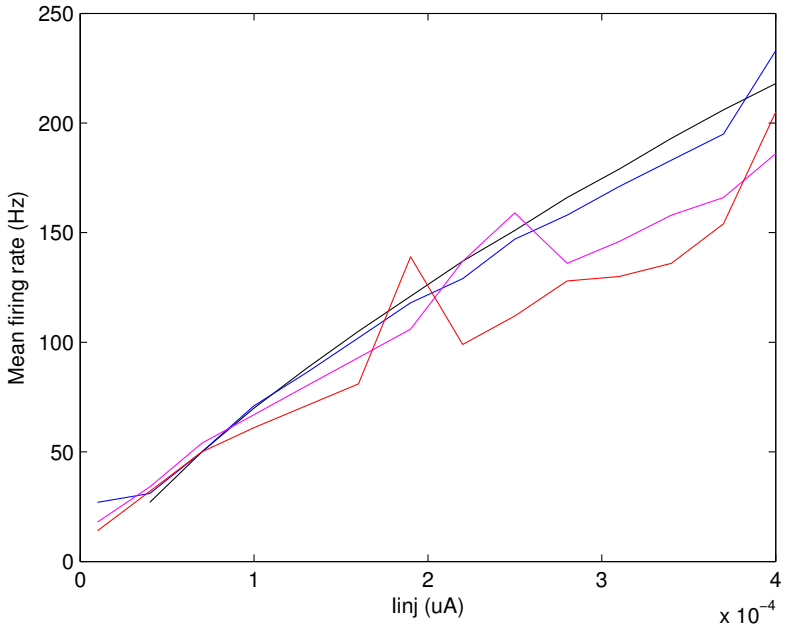

Figure 2.2: Frequency versus stimulation current f(i) curves of FS neurons with different σ: $\sigma = 0$(black curve), $\sigma = 0.01$(blue curve), $\sigma = 0.02$(magenta curve) and $\sigma = 0.03$(red curve).

by equation 2.14) , we observe mainly two events. The first is the normal firing, as shown in Figure 2.3, that produces the realistic action potential. In Figure 2.3(a), the membrane voltage oscillations are the dominant effect of the stochastic nature of ion channel, with spontaneous spiking. In Figures 2.3(c) and 2.3(e), the supra-threshold stimulation currents result with irregular spiking, occasional missing spikes and membrane voltage oscillations. The second is the linear f(I) curve with small depolarizing currents curve that is produced from the normal firing, as shown in Figure 2.2. This linear f(I) curve is obtained by the superposition of different firing rate, that is in function of the current, and it is modulated by σ that represents the amplitude of the noise. In Figure 2.2, the HH model is affected by noise, it has a firing rate with lower frequencies due to random subthreshold oscillations, occasional spontaneous spikes, and clusters of action potentials.

For CPR neuron the time constants used are: $C_{\tau,m}$=3 for m, $C_{\tau,h}$=50 for h, $C_{\tau,n}$=20 for n, $C_{\tau,o}$=2500000 for o and $C_{\tau,s}$=20000 for s. As we can see the constants for the slow conductances (I_{slowK} and l_{slowNa}) are big: this means that the amplitude of the noise is

very big compared to the signal, then the membrane voltage that we obtain is too noisy and the neuron can with difficulty overcome the threshold voltage and obtain a neural activity. Moreover the conductances that realize the formation of action potential are leakeage, sodium and postasium, instead the slow conductances have only the function of adaptation of the action potential: as we can see by Figure 3.9 their effects can be considered finished after $40s$. So to create a stochastic neuron, we have to make the opening and closing of ion channels noisy that determine the action potential. Then we add the noise only into the leakeage, sodium and postasium conductances. However we have a stochastic behaviour of the CPR neuron although we don't add noise in slow conductances because the other conductances with noise make the stochastic membrane voltage that in turn affects the slow conductances. In the table 2.1 we summarize the values of the constant C_τ to obtain the HN, IN and CPR stochastic neurons.

neuron type	**conductance type**	**value** C_τ
HN	m	3
	h	50
	n	20
IN	m	3
	h	50
	n	20
CPR	m	3
	h	50
	n	20
	o	0
	s	0

Table 2.1: Constant values (C_τ) to achieve the HN, IN and CPR stochastic neurons

.

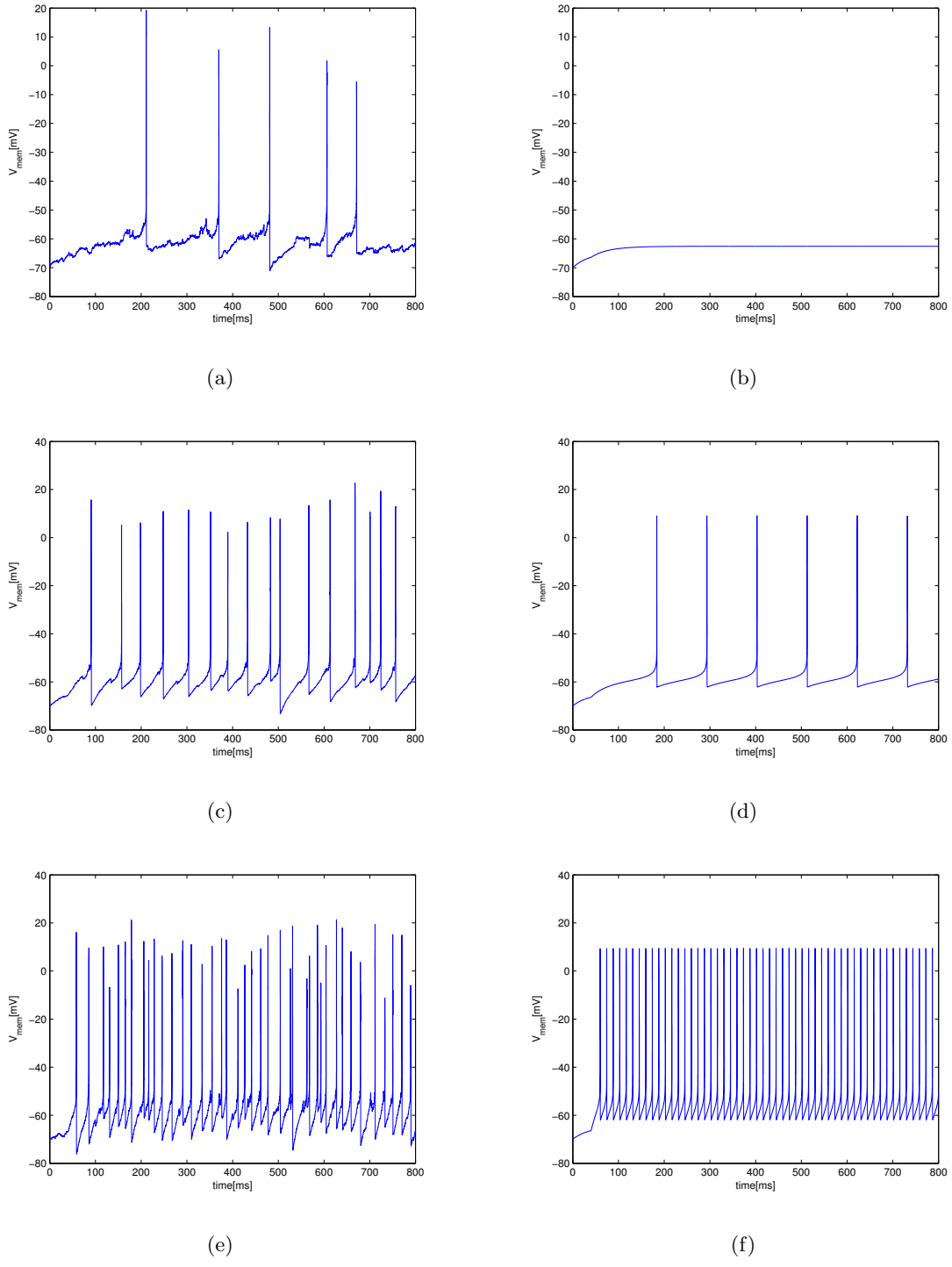

Figure 2.3: Comparison between the reponses obtained by the deterministic (right panels) and stochastic models (left panels) in reponse to three different depolarizing current. For the stochastic trace $\sigma = 0.03$. The traces 2.3(a) and 2.3(b) are stimulated with $I = 0.008nA$. The traces 2.3(c) and 2.3(d) are stimulated with $I = 0.02nA$. The traces 2.3(e) and 2.3(f) are stimulated with $I = 0.1nA$.

Chapter 3

Modeling of CPR Network

This network is called CPR due to the name of one of the main neurons that are comprised in the biological network. The circuit interests us in the switch-like behaviour, which seems to spike in response to a certain kind of stimuli. From the biological experiments data we construct a network model that emulates the same physiological behaviour, according to the HH model. In this chapter, we first introduce the electrophysiological phenomena of CPR biological network. In the following section, we present as these phenomena are reproduced in our model. Results of Matlab simulations on the HN, IN and CPR neurons and synapses that support the correctness of this model are reported.

3.1 Biology CPR Network

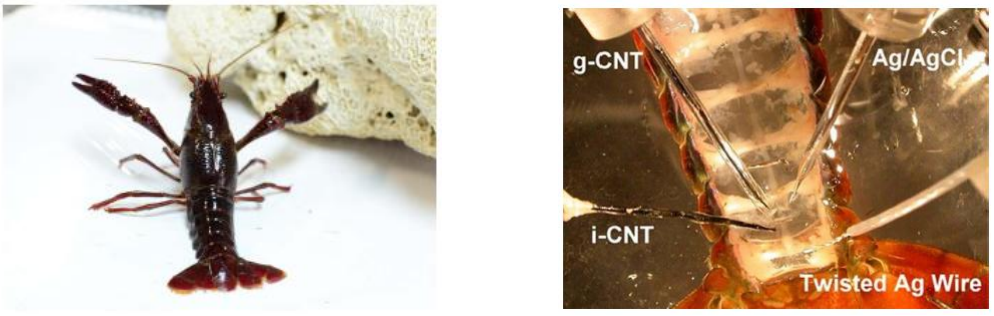

(a) (b)

Figure 3.1: (a) A crayfish [20]. (b) The setup of neuron measurement [20].

The crayfish is a kind of small lobsters shown in Figure 3.1 (a). To measure neuron signals, our colleague from NTHU dissect the crayfish and we pay attention just to the

abdominal nerve cord (a number of nerves) and then the Ag/AgCl electrode is introduced to record neural signals, as shown in Figure 3.1 (b).

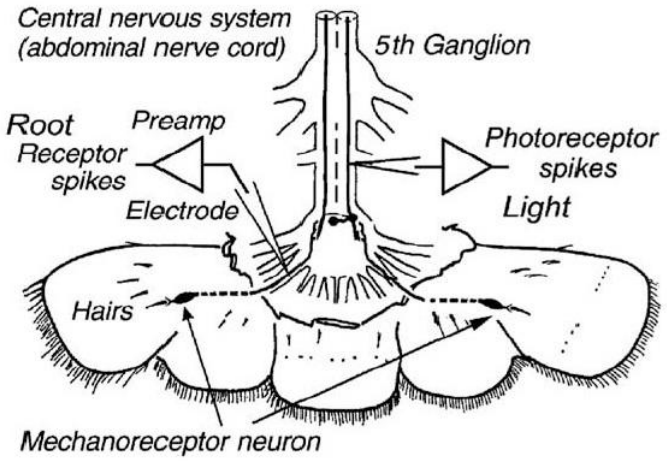

Figure 3.2: The anatomy of the tail of a crayfish [21].

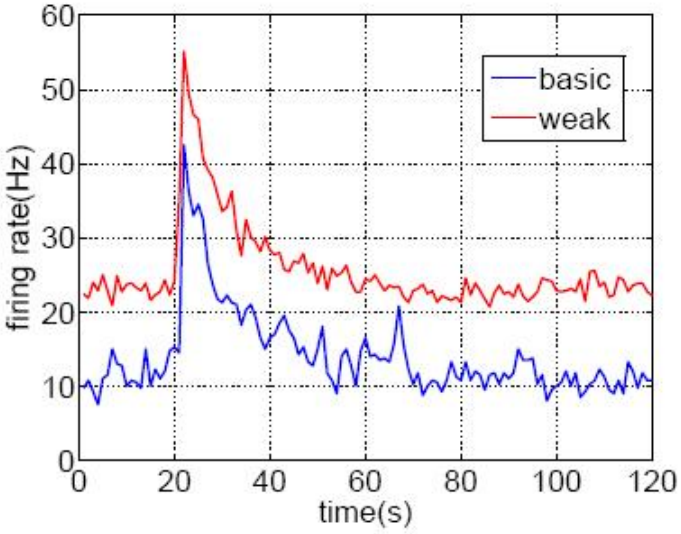

Figure 3.3: The blue line is the firing-rate curve of the CPR neuron with a 1s (20s∼21s) stimulus (blue line). The red line shows the wave enhancement phenomenon [20].

The recording method can be either intracellular or extracellular, depending on whether the electrode is put either inside or outside the neuron. In our experiments, the extracellular recording is used and the amplitude of the measured action potentials is around 1mV. The CPR model is mainly located in the tail of a crayfish as shown in Figure 3.2. To use a more quantitative method for describing biological phenomena, we analyze the

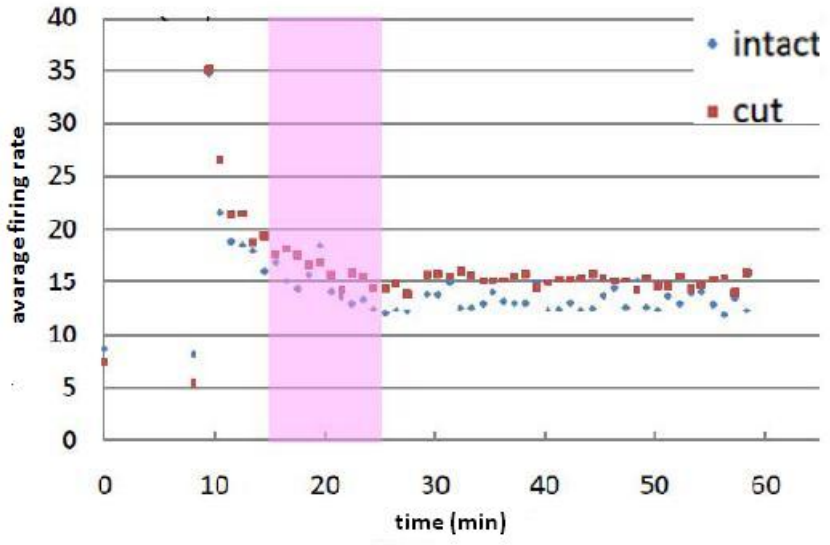

Figure 3.4: The afferent-cut phenomenon. The blue point is the firing rate before the removal of the afferent nerve and the red point is after the removal. The stimulus is a continuously constant stimuli applied to the CPR neuron and start at 10min [20].

mean firing rate which is defined as the number of action potentials occurring within each one-second window. The firing rate of CPR neurons exposed to an optical stimulus for one second is shown in blue line in Figure 3.3. We can see that this curve increases when the stimulus is applied. To investigate how the two types of sensory neurons (CPR neurons and hair neurons) interact, we apply stimuli to them simultaneously. In the experiment, the CPR neuron is stimulated with an optical source (LED) for one second and machines are used to generate water wave or electrical stimuli to the hair neuron.

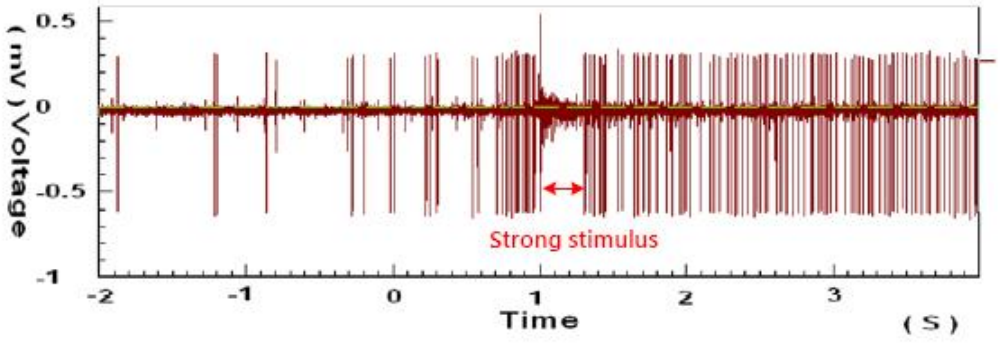

Figure 3.5: The inhibition induced by an electrical shock. The CPR neuron stops firing when a strong stimulus is applied to the HN [20].

The experimental data show that the CPR neurons change the firing rate in opposite

directions when distinct stimulus strength is applied to the hair neurons. If the strength is weak such as water wave, the firing rate of the CPR neuron will increase as shown in red line in Figure 3.3. On the other hand, Figure 3.5 shows that the CPR neuron will stop firing, if the stimuli are strong, such as a direct electrical stimulus. We call the first phenomenon the wave enhancement and the second one the inhibition induced by an electrical shock. Now, another phenomenon is observed: if we cut the afferent nerve, we eliminate the signals from the hair neuron; this increases of the firing rate and seems to indicate that the hair neuron has an inhibitory effect on the CPR neuron, as shown in Figure 3.4. The latter phenomenon can be observed in Figure 3.6: if one of the CPR neurons is excited, it will inhibit accordingly another CPR neuron and vice versa. We call it mutual inhibition and oscillation.

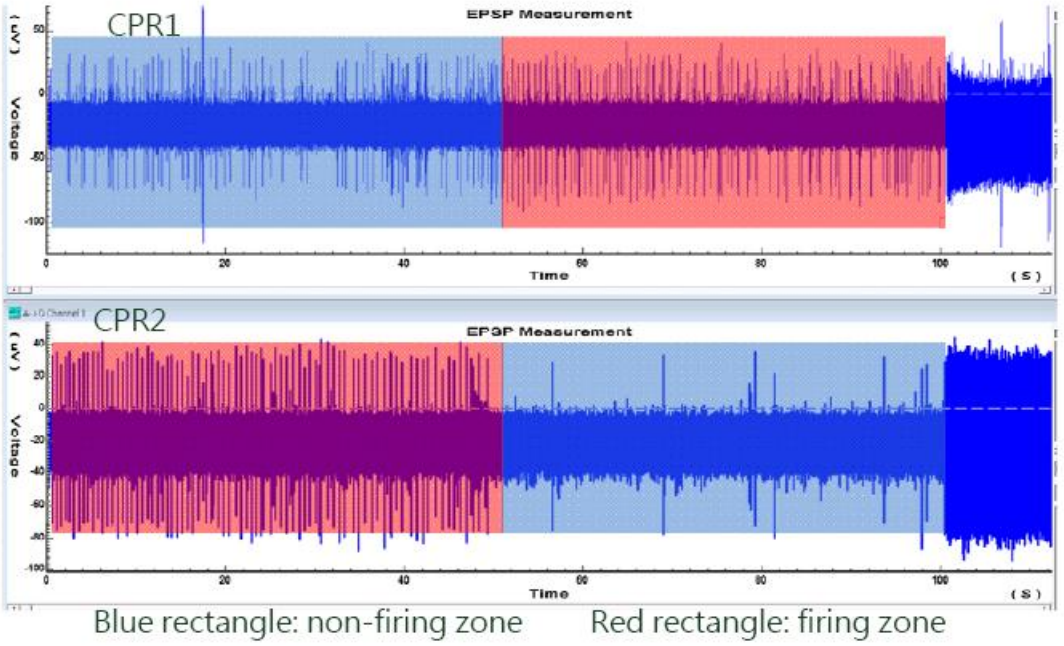

Figure 3.6: The mutual inhibition and oscillation between the CPR neurons [20].

3.2 CPR network model

To model the physiological behaviour of the tail of the crayfish in our CPR network , that is proposed by NTHU [20], there are 2 CPR neurons, 2 HN neurons, 2 IN neurons and 12 synapses (S1 S2 S3 S8 S9 S10 are equal to S4 S5 S6 S7 S11 S12), as shown in figure 3.7. The four electrophysiological phenomena that we saw in the previous section are modeled in such CPR Network:

- wave enhancement is modeled by the connection between the HN and CPR with synapse S1 (S2). When a weak stimulus is applied to the HN, the stimulus strength is not strong enough to make the IN fire. Thus, the firing rate of the CPR neuron will be increased by the current of the excitatory synapse S1 (S5).

- Induced inhibition is modeled by the chain which is formed by the HN, IN, CPR and the synapses between them. The IN is excited by the synapse S2 (S6) and fires. As soon as the IN fires, there is a current drawn from the CPR neuron through the inhibitory synapse S3 (S7). Although the synapse S1 (S5) still works and increases the excitability of the CPR neuron, the weight of the inhibitory synapse S3 (S7) is larger (in fact the value of the synapse g_{syn} S3 is bigger than S1), resulting in the inhibition of the CPR neuron. Thus the IN acts as a switch and modulates the firing-rate of the CPR neuron under distinct levels of stimulus strength.

- Afferent-cut phenomenon is modeled by the cross-connected synapses, from the left HN to the right CPR2 and from the right HN to the left CPR1. Although there are two synapses, one excitatory and one inhibitory S1, S4 (S5, S8), connected to the same CPR neuron, we can adjust the weight of the inhibitory synapse. In this way we aim to give it a more relevant contribution in the case of a very weak stimulus (it can be seen as no stimulus) applied to both HNs. By this one, the CPR neuron will be slightly inhibited under the condition mentioned above when the afferent one is intact. If the afferent nerves are removed, the synapses S1, S2, S4 (S5, S6, S8) will be no more functional and the firing rate will increase, causing the afferent-cut phenomenon.

- The mutual inhibition and oscillation is modeled by the four synapses S9, S10 (S11, S12) between the two CPR neurons. The inhibitory synapses have smaller time constants than the excitatory ones. When a CPR neuron is inhibited, it will fire again because of the slowly-increasing current of the excitatory synapse. As soon as it fires, the other CPR neuron is inhibited and repeats the procedure.

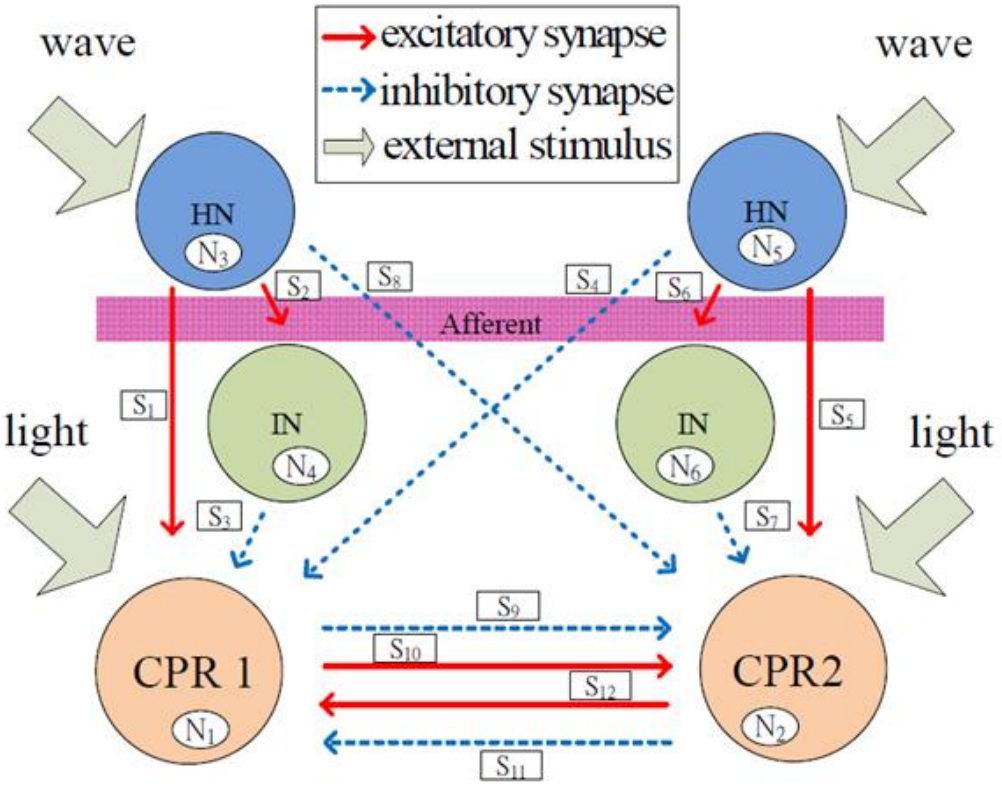

Figure 3.7: The CPR network model [20].

3.2.1 CPR neuron

The first neuron that we analyze is the CPR neuron one. As we can see from firing rare which is a bell-shaping curve (as shown in Figure 3.8 b), it is not constant but varies under the stimulus.

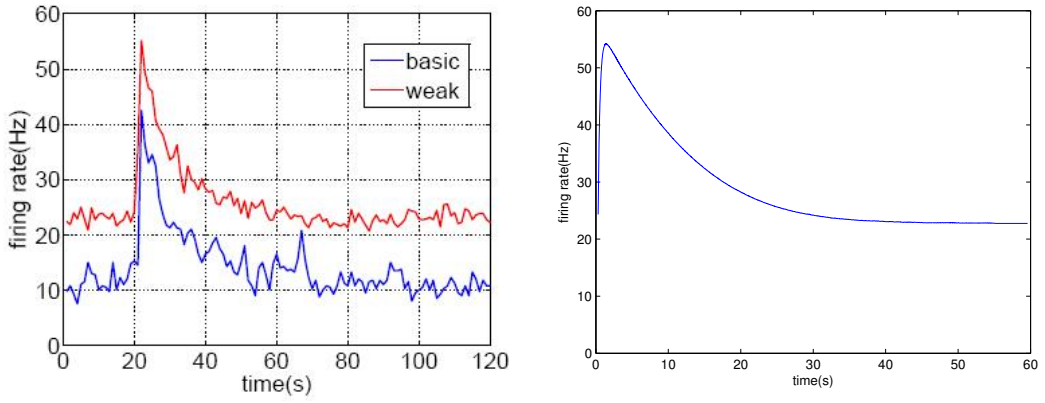

(a) (b)

Figure 3.8: (a) Biological Firing-rate curve of the CPR [20]. (b) Firing rate of the CPR neuron with $I_{ext} = 0.0008nA$..

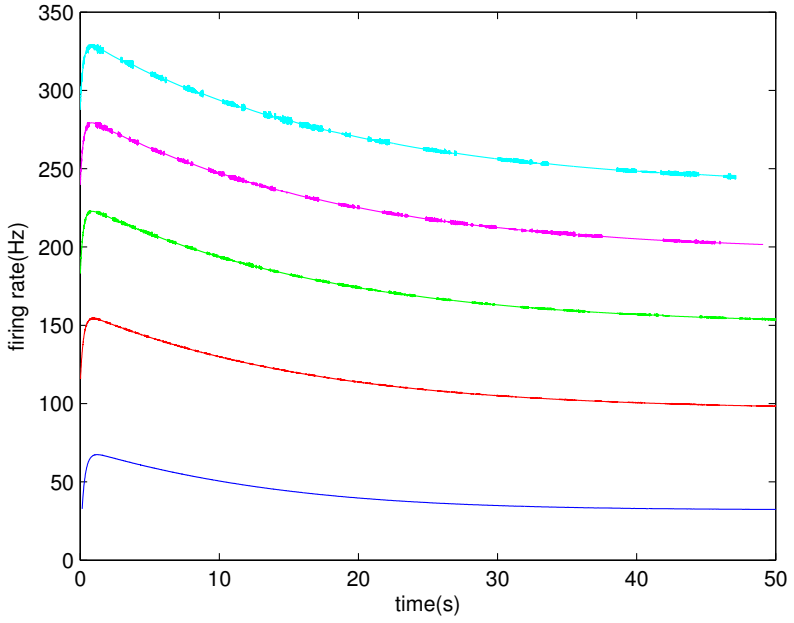

Figure 3.9: Firing rate of the CPR neuron with I_{ext}=0.01nA(b), I_{ext}=0.1nA(r), I_{ext}=0.2nA(g), I_{ext}=0.3nA(m) and I_{ext}=0.4nA(c).

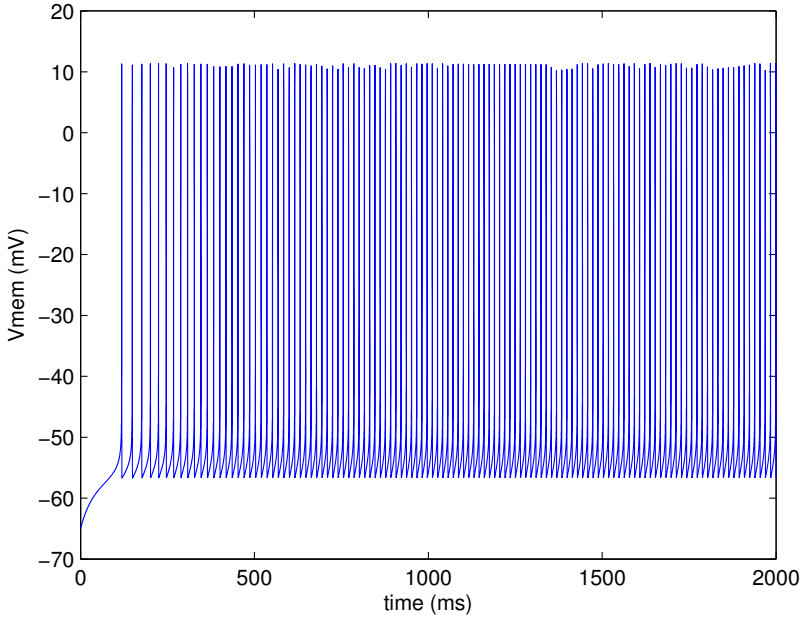

Figure 3.10: Membrane potential of the CPR neuron with stimulation current I_{ext}=0.01nA

This indicates that there is an ion channel slowly injecting currents into the membrane. In fact, for a very large firing rate, we can note an increasing phase, a decreasing one and then a settle to a fixed value. Hence, the CPR neuron is modeled as a RS neuron (with a leakage, a sodium, a potassium and a slow ion channel, as channel modulation) but in this case we add two slow ion channels. One of them is $I_{slow,Na}$, which slowly injects currents to the membrane. The other one, $I_{slow,K}$, also influences the membrane voltage, but in delay. In Table 3.1 we can see the composition of the ionic current of the CPR neuron. The biological parameters of CPR neuron, are summarized in Table 3.2, with them we

ion current	**ion type**	**gating kinetics**
I_{Na}	Na^+	m^3h
I_K	K^+	n^4
$I_{slow,Na}$	Na^+	s
$I_{slow,K}$	K^+	o

Table 3.1: Extracted parameters of the composition of the ionic current of the CPR neuron

obtain the firing rate of Figure 3.8 b. In Table 3.1, we can see the composition of the ion current of CPR neuron. From the composition of the Figure 3.8 we can observe that the firing rate simulated in MATLAB, it has the same red line pattern of biological recording.

To get the current stimulation of our CPR neuron, in MATLAB, the neuron is stimulated with different values of current. Then the instantaneous frequency of each spike during $50s$ is calculated for each different values of stimulation current, thus obtaining the graph in Figure 3.9. We induce a stimulation current of $0.01nA$ so we get a frequency of 35Hz at the end of the transient. We are not going to lower frequencies because the stimulation current is already low and no lower one can be generated due to technological limits. In Figure 3.10, we can observer that the period of the first spikes of the membrane potential are great respect those following, according to the firing rate in the Figure 3.8 b.

3.2.2 The HN and IN neurons

The mechanoreceptor hair cells (HN) is a neuron that behaves like a simple FS neuron and consists of leakage, sodium and potassium channel. In fact, we introduced another FS neuron in order to model correctly the phenomena of biological networks CPR. The wave enhancement and the inhibition induced by an electrical shock result from the existence of the inter-neurons(IN). The IN neuron has the same parameters of the HN neuron (as shown in Table 3.2). In the Figure 3.11 we can observe the firing-rate of HN and IN neurons. You can see that we must apply a stimulation current of 0.05nA, if we want a realistic neuron frequency of about 35Hz.

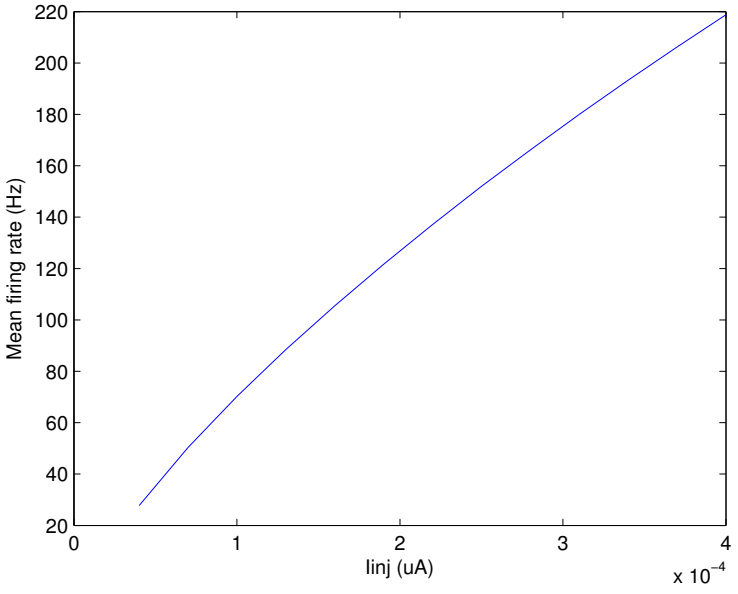

Figure 3.11: Firing-rate curve of FS neurons

	HN neuron	IN neuron	CPR neuron
$C_M(\mu F/cm^2)$	1	1	1
$g_{Na}(mS/cm^2)$	40	40	40
$E_{Na}(mV)$	30	30	30
$\tau_m(ms)$	0.03	0.03	0.03
$V_{offset,m}(mV)$	-40	-40	-37.3
$V_{slope,m}(mV)$	5.5	5.5	5.5
$\tau_h(ms)$	0.5	0.5	0.5
$V_{offset,h}(mV)$	-45	-45	-42
$V_{slope,h}(mV)$	4	4	4
$g_K(mS/cm^2)$	35	35	35
$E_K(mV)$	-80	-80	-80
$\tau_n(ms)$	0.2	0.2	0.2
$V_{offset,n}(mV)$	-40	-40	-35
$V_{slope,n}(mV)$	7.5	7.5	7.5
$g_{mS/Leak}(cm^2)$	0.03	0.03	0.03
$E_{Leak}(mV)$	-64,9	-64.9	-60
$g_{slowNa}(mS/cm^2)$			0.04
$E_{slowNa}(mV)$			30
$\tau_{slowNa}(ms)$			200
$V_{offset,s}(mV)$			-37.5
$V_{slope,s}(mV)$			5.5
$g_{slowK}(mS/cm^2)$			1.5
$E_{slowK}(mV)$			-80
$\tau_o(ms)$			25000
$V_{offset,o}(mV)$			0
$V_{slope,o}(mV)$			2.5

Table 3.2: Parameters of biological HN, IN and CPR neurons

3.2.3 The synapse in the CPR network

To describe the synapse in the CPR network we use the equations 1.8, 1.9 and 1.10 defined by the synaptic model of the previous chapter. In this network E_{syn} is 20mV for excitatory

synapses and -80mV for inhibitory synapses and the biological parameters of synapses, are summarized in Table 3.3.

	Syn (1-5)	**Syn (2-6)**	**Syn (3-7)**	**Syn (4-8)**	**Syn (9-11)**	**Syn (10 -12)**
$g_{syn}(mS/cm^2)$	0.08	0.12	20	0.02	0.7	0.2
$E_{syn}(mV)$	20	20	-80	-80	-80	20
$\tau_{syn}(ms)$	1	1	1	1	100	1000
$V_{syn}(mV)$	-30	-10	-20	-28	-30	-30
$V_{syn}(mV)$	1	2	3	15	2	3

Table 3.3: The biological parameters of the synapses

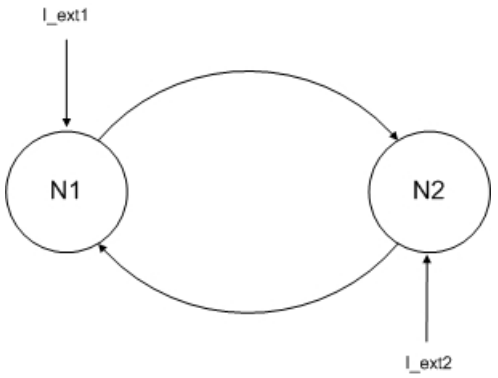

Figure 3.12: A single neuron oscillator

Another of our goals is to find a possible hardware implementation for synapses. From equation 1.8 it can be seen that it is similar to the equation of the potassium current, except for the gating variable of the synapse that is power one instead of the potassium one, which is four. Therefore we decided to implement the equations of synapses in Simulink as those of the potassium current by changing only the power of the gating variable. To test the functioning of neural synapses, we use the principle of the oscillator. A neural oscillator consists of a feedback loop between a couple of neurons, as illustrated in Figure 3.12. This technique is the first test that is performed to verify that the communication between neurons is working. If neurons influence each others, in accordance with their inhibiting or exciting nature, communication works, and so more neurons can be involved in the network. In this case, to test the synapse we use the only link between the neuron one to two, with the synapse between the two neurons, as shown in Figure 3.13.

As long as six to twelve synapses have got the same values, it is possible to run the simulation using six of them, i.e. S1, S2, S3, S8, S9 and S10. We impose a fixed current

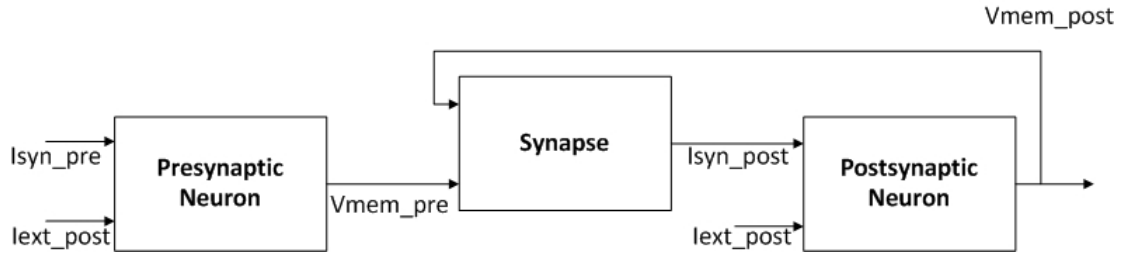

Figure 3.13: Block diagram for testing the synapse

$I_{ext_{pre}} = 0.2nA$ to the presynaptic neuron, instead $I_{ext_{post}} = 0.05nA$ to the postsynaptic one. To see if the synapse is excitatory or inhibitory, we perform two tests for each synapse: through the first we analyze the behaviour of the postsynaptic membrane potential at rest (stimulated by a current $I_{syn_{post}} = 0nA$) and then we consider the postsynaptic membrane potential with the $I_{syn_{post}}$ generated from the synapse. If the postsynaptic membrane voltage increases, it means that the synapse is excitatory; on the contrary, if it decreases it means that it is inhibitory. As can be seen from the simulations in Simulink, synapses S1, S2, S11 are excitatory (Figures 3.14, 3.15 and 3.16) while S3, S8, S10 (Figures 3.17, 3.18 and 3.19) are inhibitory. It is very important to note that synaptic current in the postsynaptic neuron must be subtracted from the equation (1.2), because the direction of reference is opposite to that of the Figure 1.7.

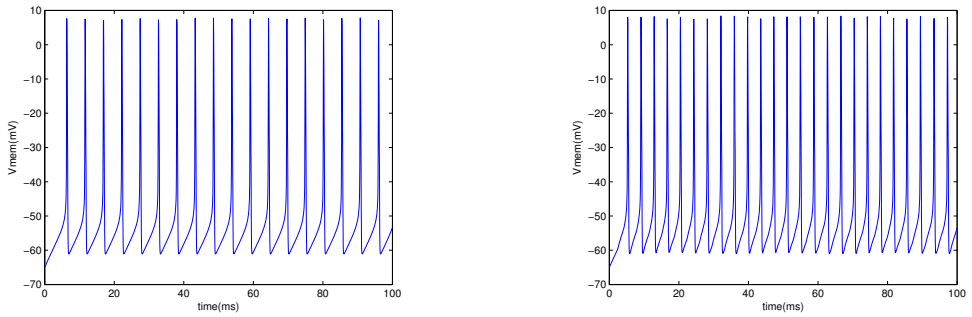

Figure 3.14: Excitatory Synapse 1 and 5: the membrane potential increases with the synaptic contribution.

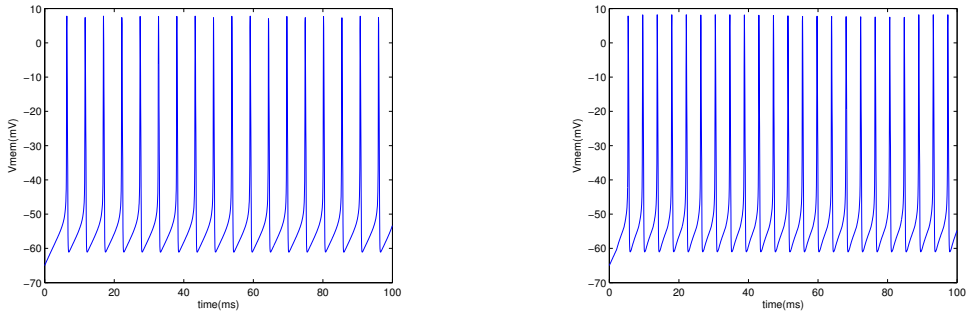

Figure 3.15: Excitatory Synapse 2 and 6: the membrane potential increases with the synaptic contribution.

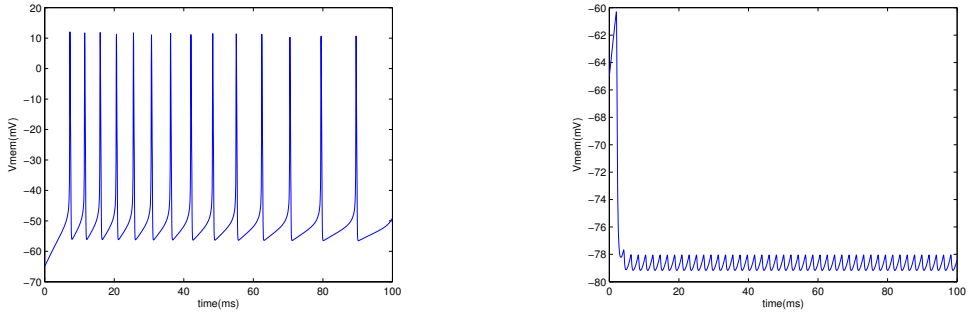

Figure 3.16: Inhibitory Synapse 3 and 7: the membrane potential decreases with the synaptic contribution.

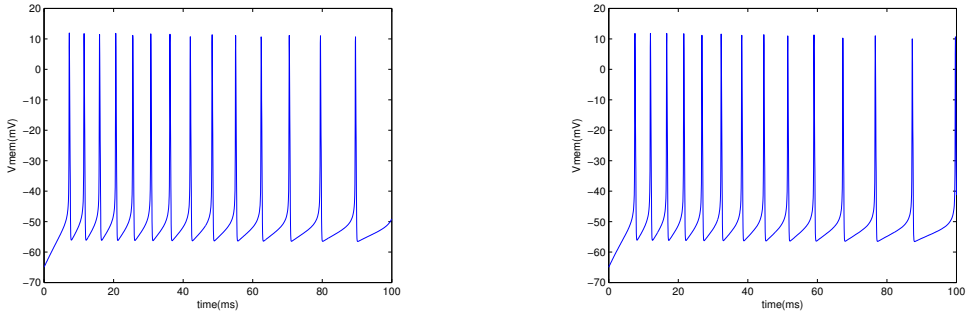

Figure 3.17: Inhibitory Synapse 4 and 8: the membrane potential decreases with the synaptic contribution.

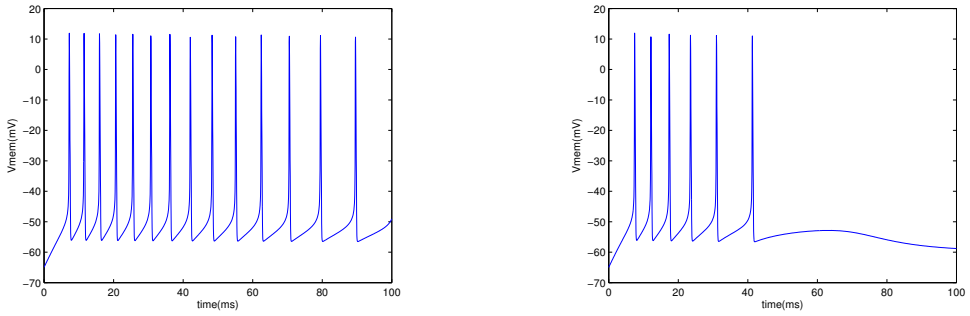

Figure 3.18: Inhibitory Synapse 9 and 10: the membrane potential decreases with the synaptic contribution

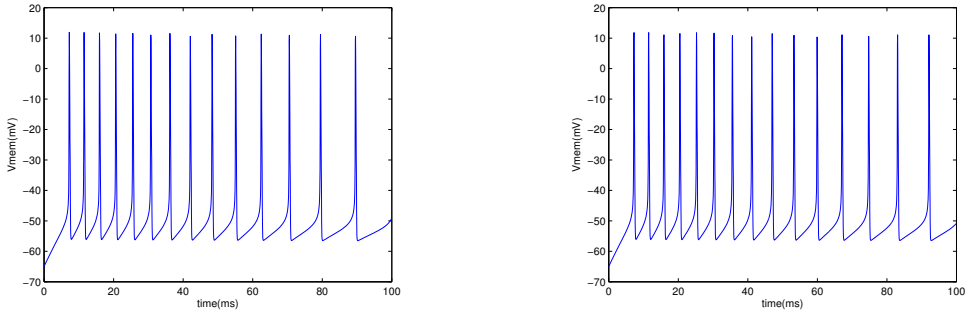

Figure 3.19: Excitatory Synapse 11 and 12: the membrane potential increases with the synaptic contribution

Chapter 4

Design CPR Network

In this chapter, we explain the design methodology of our chips in particular we analyze the properties of its noise immunity. In the following we describe an analog library of mathematical operators [23], according to the HH formalism, developed in the previous Galway chip of the research team, which we readapt to realize the neurons in CPR Network.

4.1 Design principle of conductance based model

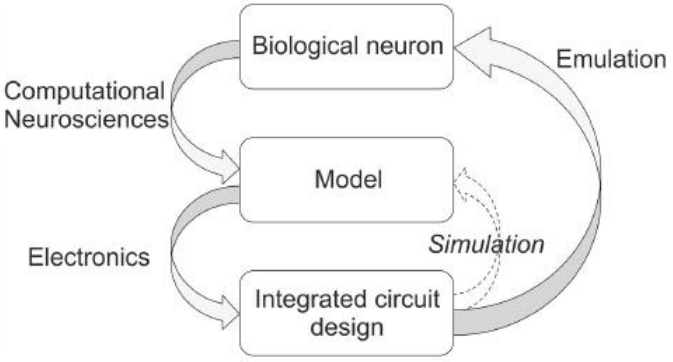

Figure 4.1: Design methodology of an integrated neuromimetic circuit [4].

To design our chip, which is called Hysnet, we use the following model for the design of analog neuromimetic ICs as shown in Figure 4.1.

The computational neuroscientists of the biological measures develop a mathematical model. Then the electronic engineers from the mathematical model realize the IC. After this, they simulate the behaviour of the chip to verify that it works properly. Finally this IC is connected to a biological system to emulate his electrophysiological behaviour

and study its interaction with biological cells. To develop this ASIC (Application Specific Integrated Circuit) we use the Cadence platform. Cadence is a graphical interface for unified management of the design flow for digital ICs, analog and mixed, which includes more than one hundred software tools, and has long been an industry standard.

Between different Cadance tools, our design is useful to use the Verilog-A language,

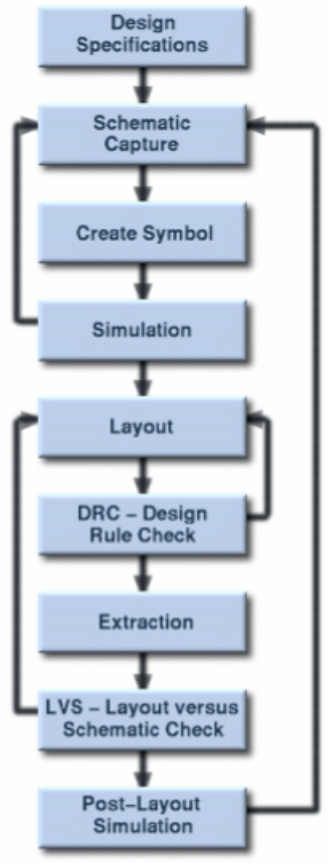

Figure 4.2: Design process flow diagram

that is a high-level language that uses modules to describe the structure and behaviour of analog systems and their components. A design flow in Cadence for standard full-custom analog circuits is shown in Figure 4.2. Hysnet chip has been designed thanks to BiCMOS 0.35 um SiGe technology of austriamicrosystems. BiCMOS technologies are hybrid and theyintegrate CMOS and BJT on the same semiconductor chip.

For our design, we retained five channel types: leakage, sodium, potassium, slow-sodium and slow-potassium. By combining those channels, we can model the HN, IN and CPR neurons described in Chapter 3. Each conductance is obtained by assembling blocks of mathematical functions according to the block diagram of ionic current generators in

Figure 4.3. We use the same principle to achieve the synapse, then it is constituted by the block diagram in Figure 4.4. For the design of synapses first we realized the different blocks by VerilogA then we replaced once with transistor blocks.

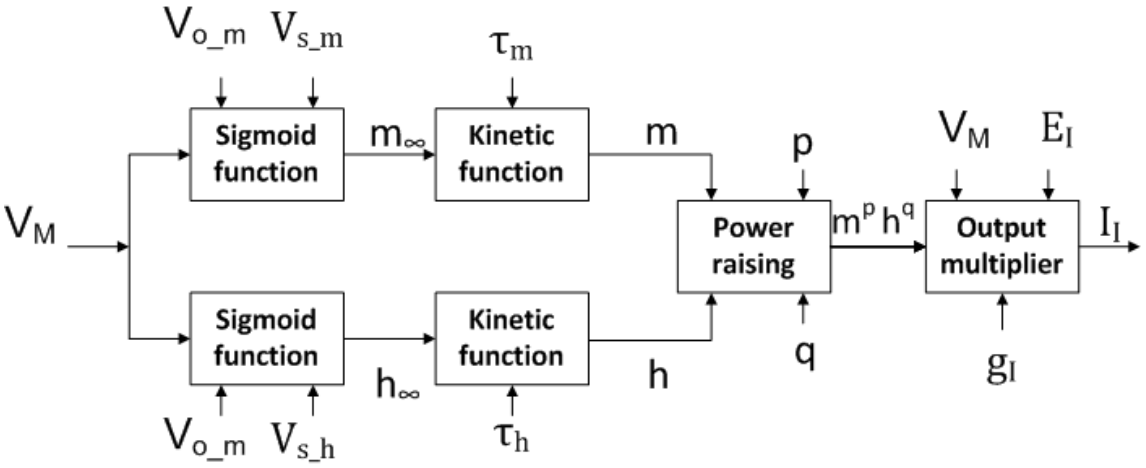

Figure 4.3: Block diagram of the ionic current generator.

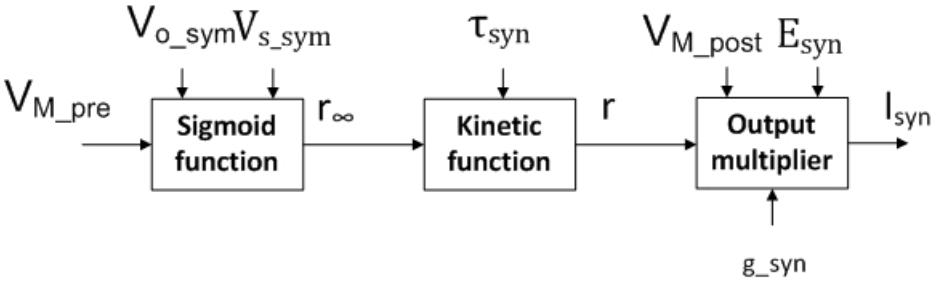

Figure 4.4: Block diagram of synapse generator.

We designed the functions in current mode, so that all of the internal variables are physically represented by currents, in order to make the design of the various easiest operations. Moreover in all functions the MOS transistors operate above threshold.

4.2 From biology to hardware implementation

In order to increase the noise immunity, we applied a x5 gain factor to the biological voltages:

$$V_{VLSI} = 5 \cdot V_{Bio} \tag{4.1}$$

This means that the action potential varies about between -320mV to 250mV.

To obtain this transition from biological to hardware implementation [4] we have to replace

in the equations of HH model V_{VLSI}, g_{VLSI} and I_{VLSI}:

$$g_{VLSI} = g_{Bio} \cdot \frac{C_{VLSI}}{C_{Bio}} \tag{4.2}$$

$$I_{VLSI} = I_{Bio} \cdot 5\frac{C_{VLSI}}{C_{Bio}} \tag{4.3}$$

C_{VLSI} and C_{Bio} represent the membrane capacitans of artificial and biological neurons. In the out chip, CVLSI = 220 nF and the biological neurons have $C_{Bio} = C_M \cdot Area$ with $C_M = 1uF/cm^2$ and Area is the neuron Area. In addition, our system provides that the parameter values for the command the ionic conductances are transmitted to the ASIC as a voltage. These parameters are shown in the table 4.1 for HN and IN neurons.

	HN neuron	**IN neuron**
$g_{Na}(V)$	3.762	3.762
$E_{Na}(V)$	2.65	2.65
$\tau_m(V)$	3.956	3.956
$V_{offset,m}(V)$	2.3	2.3
$V_{slope,m}(V)$	4.175	4.175
$\tau_h(V)$	4.373	4.373
$V_{offset,h}(V)$	2.275	2.275
$V_{slope,h}(V)$	4.4	4.4
$g_K(V)$	3.917	3.917
$E_K(V)$	2.1	2.1
$\tau_n(V)$	3.433	3.433
$V_{offset,n}(V)$	2.3	2.3
$V_{slope,n}(V)$	3.875	3.875
$g_{Leak}(V)$	4.833	4.833
$E_{Leak}(V)$	2.796	2.796

Table 4.1: Parameters of Hardware HN and IN neurons

4.3 Elementary circuits for neural analog functions

In this section we present the elementary circuits required for obtaining the analog neural functions to achieve neurons and synapses depending on the HH model.

4.3.1 Voltage-current converter

The model's parameters are applied to the chip in the form of voltages. Since we chose to use a current mode design, then it becomes necessary to have voltage-current converters (VCC). The solution with a high linear range uses one operational amplifier, one resistor, and one MOS transistor, and it is shown in Figure 4.5. The usage of a polysilicon resistance, unlike resistors implanted in silicon, will present the advantage of being linear over the range of operating voltage. We then obtain the following linear relationship:

$$I_O = -\frac{Vcc - Vi}{R_{Conv}} \tag{4.4}$$

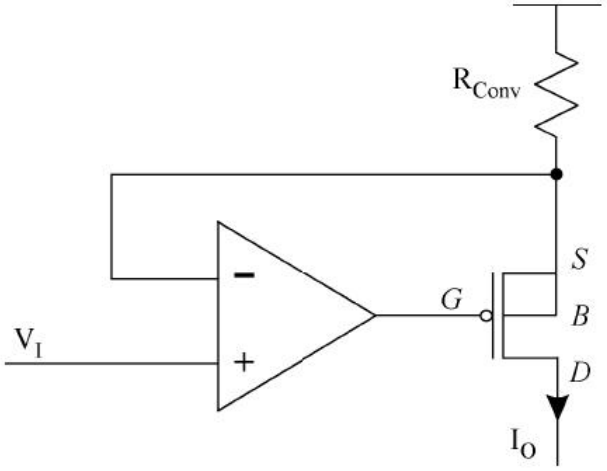

Figure 4.5: Voltage-current converter using 1 op-amp, 1 PMOS transistor and 1 resistor (V_i is the input and I_O is the output)[23].

4.3.2 Current-mode multiplier

The current used in our ASIC design offers simple solutions to make the operations of addition and subtraction. To perform multiplication or division, you must use more elaborate circuits. In our model, the input variables are the activation and inactivation terms (1.3), and these terms are bounded by 0 and 1, then we can use only a single one-quadrant multiplier, as shown in Figure 4.6.

This structure uses the translinear principle that says: in a closed loop containing an even number of translinear elements (TEs) with an equal number of them arranged clockwise and counter-clockwise, the product of the currents through the clockwise TEs

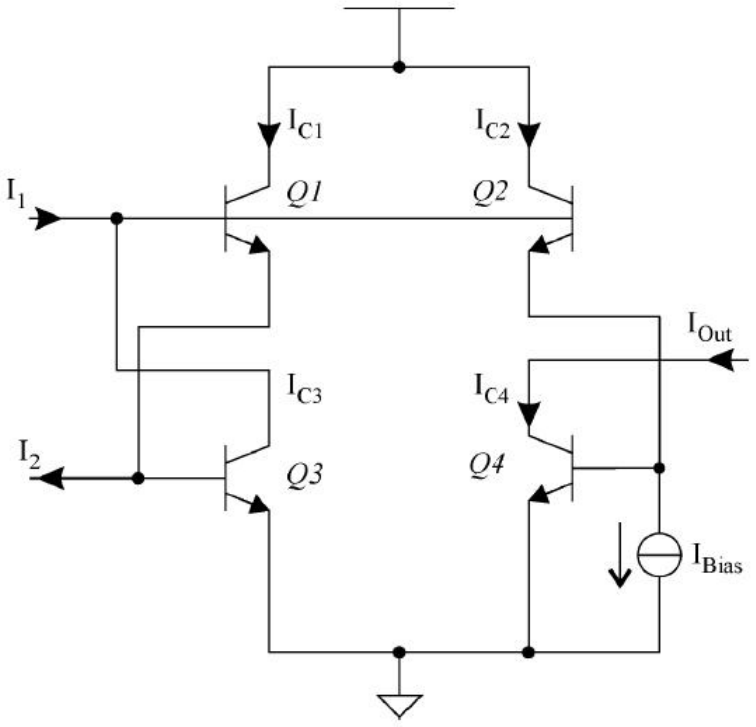

Figure 4.6: One-quadrant multiplier in current mode using the NPN transistor with $I_{C_1} \cdot I_{C_2} = I_{C_3} \cdot I_{C_4}$,resulting in $I_{Out} = I_1 \cdot I_2 / I_{Bias}$ [23].

equals the product of the currents through the counter-clockwise TEs. By Kirchoff's Voltage Law applied to the circuit in Figure 4.6 we can write:

$$V_{BE3} + V_{BE1} - V_{BE2} - V_{BE4} = 0 \tag{4.5}$$

Recalling the simplified equation of the voltage-current relationship of a bipolar transistor:

$$V_{BE} = U_T ln \frac{I_C}{I_S} \tag{4.6}$$

Substituting V_{BE} in equation 4.5 we obtain:

$$\begin{aligned} U_T ln \frac{I_{C_1}}{I_{S_1}} + U_T ln \frac{I_{C_3}}{I_{S_3}} &= U_T ln \frac{I_{C_2}}{I_{S_2}} + U_T ln \frac{I_{C_4}}{I_{S_4}} \\ ln \frac{I_{C_1}}{I_{S_1}} \frac{I_{C_3}}{I_{S_3}} &= ln \frac{I_{C_2}}{I_{S_2}} \frac{I_{C_4}}{I_{S_4}} \\ \frac{I_{C_1}}{I_{S_1}} \frac{I_{C_3}}{I_{S_3}} &= \frac{I_{C_2}}{I_{S_2}} \frac{I_{C_4}}{I_{S_4}} \end{aligned} \tag{4.7}$$

Using the same transistors surface, we have:

$$I_{S_1} = I_{S_2} = I_{S_3} = I_{S_4} \tag{4.8}$$

Then the equation 4.7 becomes:

$$I_{C_1} \cdot I_{C_3} = I_{C_2} = I_{C_4} \tag{4.9}$$

The technology used and the mode of operation of the transistors allow us to simplify usual $I_B << I_C$. Thus, after identifying current I_{C_1}, I_{C_2}, I_{C_3} and I_{C_4} respectively I_2, I_{Bias}, I_1 and I_{OUT}, we get he following result:

$$I_{OUT} = \frac{I_1 \cdot I_2}{I_{Bias}} \tag{4.10}$$

4.3.3 Operational transconductance amplifier

Integrated electronic circuits have the disadvantage of having passive components very large compared to the active components. Often it is preferable to realize the function of a passive component, with the use of active components. A typical example is the integration of a high resistance value using a transconductance amplifier, as shown in Figure 4.7. To

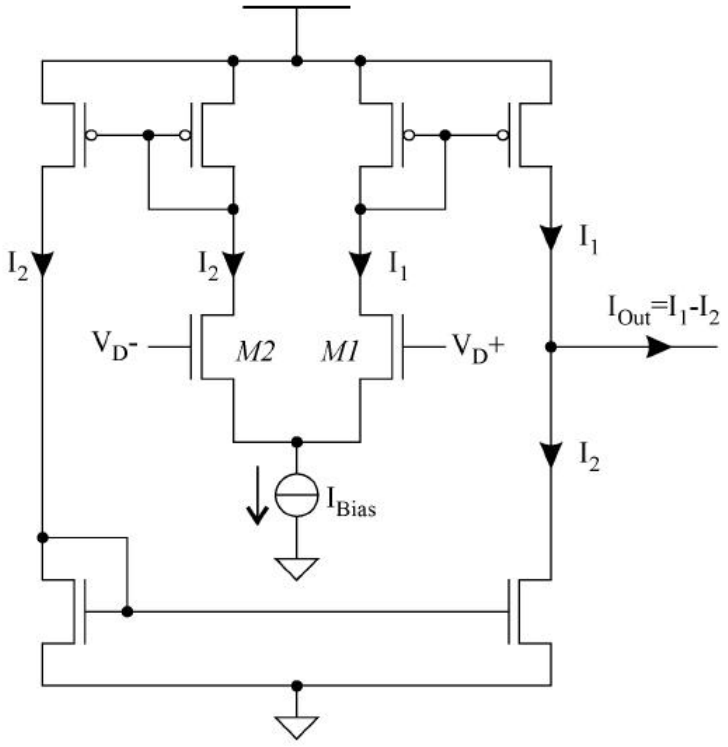

Figure 4.7: OTA, with an input V_D and an output I_{Out} [23].

emulate the behaviour of resistance, the transconductance amplifier must operate in the linear region, such as Ohm's law. Therefore, it is necessary that the MOS differential pair

$M_1 - M_2$ has a difference $I_1 - I_2$ current proportional to the control voltage V_D. Applying the Kirchhoff's current law to the source of transistors M1-M2, we obtain:

$$I_{Bias} = I_1 + I_2 \tag{4.11}$$

Applying the Kirchoff's Voltage Law to the gates of transistors M1-M2, we have:

$$V_D = V_{GS1} - V_{GS2} \tag{4.12}$$

The simplified equation of the MOS transistor in saturated linking drain current to the voltage gate is:

$$I_d = \frac{K}{2}(V_{GS} - V_T)^2 \tag{4.13}$$

where $K = \mu \cdot C_{ox} \cdot W/L$. This formula 4.30 we can write:

$$V_{GS} = \sqrt{\frac{2 \cdot I_D}{K}} + V_T \tag{4.14}$$

Assuming that the transistors M1 and M2 are identical and fusing equation (4.12) in equation 4.14, we obtain:

$$V_D = \sqrt{\frac{2 \cdot I_1}{K}} + V_T + \sqrt{\frac{2 \cdot I_2}{K}} + V_T$$
$$V_D^2 = \frac{2 \cdot I_1}{K} + \frac{2 \cdot I_2}{K} - 2\sqrt{\frac{2 \cdot I_1}{K}}\sqrt{\frac{2 \cdot I_2}{K}}$$
$$V_D^2 = \frac{2 \cdot I_{Bias}}{K} - \frac{4}{K}\sqrt{I_1 \cdot I_2}$$
$$\sqrt{I_1 \cdot I_2} = \frac{I_{Bias}}{2} - \frac{KV_D^2}{4}$$
$$\sqrt{I_1(I_{Bias-I_1})} = \frac{I_{Bias}}{2} - \frac{KV_D^2}{4}$$

$$I_1^2 - I_1 \cdot I_{Bias} + \left(\frac{I_Bias}{2} - \frac{KV_D^2}{4}\right) = 0 \tag{4.15}$$

By solving the quadratic equation in I_1 we find the following two solutions:

$$\begin{cases} I_1 = \frac{I_Bias}{2} + \frac{I_Bias}{2} \cdot V_D\sqrt{\frac{K}{I_{Bias}} - \frac{K^2 \cdot V_D^2}{4 \cdot I_{Bias}}} \\ I_2 = \frac{I_Bias}{2} - \frac{I_Bias}{2} \cdot V_D\sqrt{\frac{K}{I_{Bias}} - \frac{K^2 \cdot V_D^2}{4 \cdot I_{Bias}}} \\ \text{with } |V_D| < \sqrt{\frac{2 \cdot I_{Bias}}{K}} \end{cases} \tag{4.16}$$

Then the output current I_{Out} of the OTA is

$$I_{OUT} = I_1 - I_2 = V_D \cdot \sqrt{\frac{K}{I_{Bias}} - \frac{K^2 \cdot V_D^2}{4 \cdot I_{Bias}^2}} = V_D\sqrt{K \cdot I_{Bias}}\sqrt{1 - \frac{K \cdot V_D^2}{4 \cdot I_{Bias}^2}} \tag{4.17}$$

To study the linearity of the circuit to ensure that behaves like a resistor, we see equation 4.33 has its tangent to the point $V_D = 0$:

$$\left.\frac{\partial I_{Out}}{\partial V_D}\right|_{V_D=0} = \sqrt{K \cdot I_{Bias}} \Rightarrow \left.\tan\left(I_{Out}\right)\right|_{V_D=0} = V_D \cdot \sqrt{K \cdot I_{Bias}} \tag{4.18}$$

The formula 4.18 allows to calculate the relative error ε

$$\varepsilon = \frac{I_{Out} - V_D \left.\frac{\partial I_{Out}}{\partial V_D}\right|_{V_D=0}}{V_D \left.\frac{\partial I_{Out}}{\partial V_D}\right|_{V_D=0}} \Rightarrow \varepsilon = \sqrt{1 - \frac{K \cdot V_D^2}{4 \cdot I_{Bias}}} - 1 \tag{4.19}$$

We fix the constraints relative error of linearity $\varepsilon = 5\%$ by setting appropriate values for W and L.

4.3.4 Bipolar differential pair with predistortion stage

For the realization of the sigmoidal function (see the equation (1.5)), in more detail the term of exponential, we need to obtain the transfer functions of the type $\Delta I = K \cdot \Delta V / I_i$ where ΔV and I_i are the input variables. For this transfer function we use a bipolar differential pair with predistortion stage as shown in Figure 4.8. To simplify the calculations, we consider the case in which the base currents of the bipolar transistors are negligible compared to their collector current and then the current transmitter are equal to the collector currents.

Applying Kirchhoff's voltage law to the mesh input that is composed of the differential voltage input V_{Mem} and V_{Offset}, the transistors Q_1 and Q_2 and the resistance R, we obtain:

$$V_{in} = V_{mem} - V_{Offset} = V_{BE1} + R \cdot I_R - V_{BE2} \tag{4.20}$$

The collector currents of the transistors Q1 and Q2 are:

$$\begin{cases} I_{C_{Q_1}} = I_{Slope} + R = I_{Slope} + \frac{V_R}{R} \\ I_{C_{Q_2}} = I_{Slope} - R = I_{Slope} - \frac{V_R}{R} \end{cases} \tag{4.21}$$

We dimensioned so that I_R is very small compared I_{Slope}, also the current collector varies little and V_{BE} is almost constant in all variations of Vi then we can say that

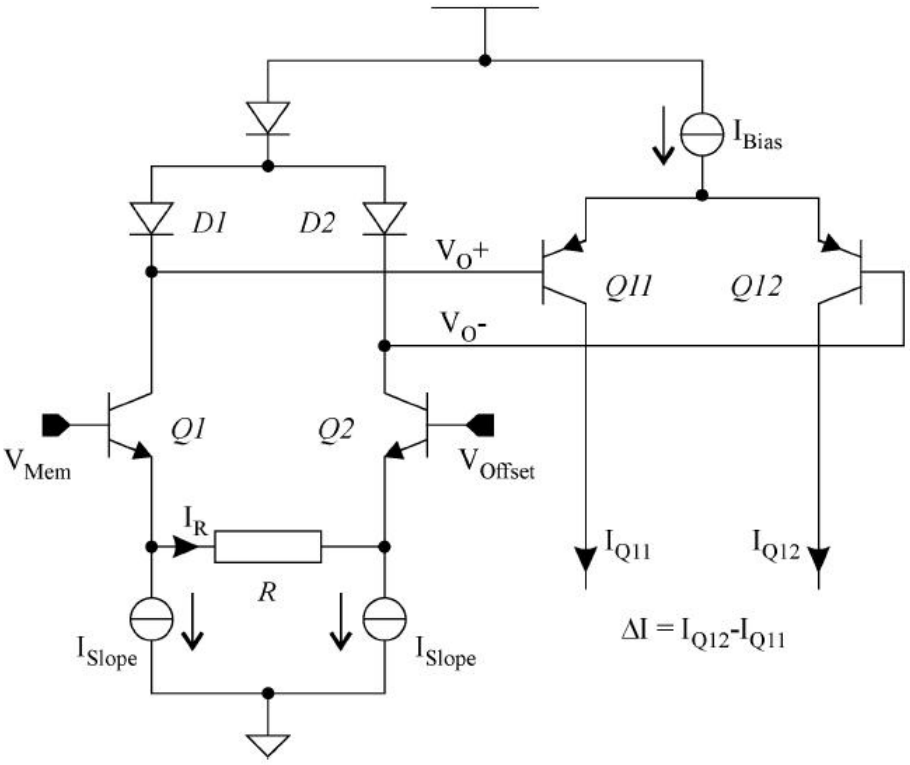

Figure 4.8: Bipolar differential pair with predistortion stage, with a differential input $V_{Men} - V_{Offset}$ and an output ΔI [23].

$V_{IN} = V_R$. The output voltage Bipolar Differential Pair is given by the difference between the voltage of the diode 1 and 2, we obtain:

$$V_O = V_{D2} - V_{D1} = U_T \cdot \frac{I_{D_2}}{I_S} - U_T \cdot \frac{I_{D_1}}{I_S} = U_T \cdot \frac{I_{D_2}}{I_{D_2}} \tag{4.22}$$

Combining the equations (4.30) and (4.22) we obtain:

$$V_O = -U_T \cdot ln \frac{I_{Slope} + \frac{V_{IN}}{R}}{I_{Slope} + \frac{V_{IN}}{R}} \tag{4.23}$$

We can write the last equation as

$$V_O = -U_T \cdot lnX \text{ with } X = \frac{I_{Slope} + \frac{V_{IN}}{R}}{I_{Slope} + \frac{V_{IN}}{R}} \tag{4.24}$$

The difference of the currents in transistors Q1 and Q2 can be written as:

$$\Delta I = I_{C_{Q_2}} - I_{C_{Q_2}} = \frac{I_{Bias}}{2}\left(1 - tanh\frac{V_O}{2 \cdot U_T}\right) - \frac{I_{Bias}}{2}\left(1 + tanh\frac{V_O}{2 \cdot U_T}\right) \tag{4.25}$$

$$= -I_{Bias} \cdot tanh\frac{V_O}{2 \cdot U_T} \tag{4.26}$$

Combining the equation (4.25) and (4.24) we obtain:

$$\Delta I = -I_{Bias} \cdot tanh \frac{-U_T \cdot lnX}{2 \cdot U_T} \tag{4.27}$$

$$\begin{aligned} \Delta I = I_{Bias} \cdot tanh \frac{lnX}{2} = I_{Bias} \frac{e^{\frac{\ln X}{2}} - e^{-\frac{\ln X}{2}}}{e^{\frac{\ln X}{2}} - e^{-\frac{\ln X}{2}}} \\ \Delta I = I_{Bias} \frac{\sqrt{X} - \frac{1}{\sqrt{X}}}{\sqrt{X} + \frac{1}{\sqrt{X}}} = I_{Bias} \frac{X-1}{X+1} \end{aligned} \tag{4.28}$$

Substituting X of equation (4.24) to the equation (4.28) we find:

$$\Delta I = \frac{I_{Bias}}{I_{Slope}} \cdot \frac{V_{IN}}{R} \tag{4.29}$$

4.4 Library of neural analog operator

In this section we describe the analog blocks that are necessary to implement the ionic conductances and synapses according to the block diagrams in the Figures 4.3 and 4.4. These analog blocks are composed of elementary circuits presented in the previous section.

4.4.1 Sigmoid function

The sigmoid block computes the steady state value corresponding to activation or inactivation terms. The Sigmoid function uses a bipolar differential pair with predistortion stage, that we have previously studied. The difference of the current ΔI in the output of bipolar differential pair with predistortion stage through the resistors r, and produces a voltage of the input differential pair composed of transistors Q3 and Q4. Using the calculations to obtain the equation (4.29), we obtain:

$$\begin{cases} I_{Inact} = \frac{I_{Sig}}{1+exp\left(\frac{r \cdot I_{Bias}}{R \cdot U_T} \frac{V_{Mem} - V_{Offset}}{I_{Slope}}\right)} \\ I_{act} = \frac{I_{Sig}}{1+exp\left(-\frac{r \cdot I_{Bias}}{R \cdot U_T} \frac{V_{Mem} - V_{Offset}}{I_{Slope}}\right)} \end{cases} \tag{4.30}$$

where I_{Inact} produces inactivation term and I_{nact} produces activation term. This term activation and inactivation is normalized between 0 and 1 in the biological model, it is in the circuit bounded between 0 and I_{Sig}.

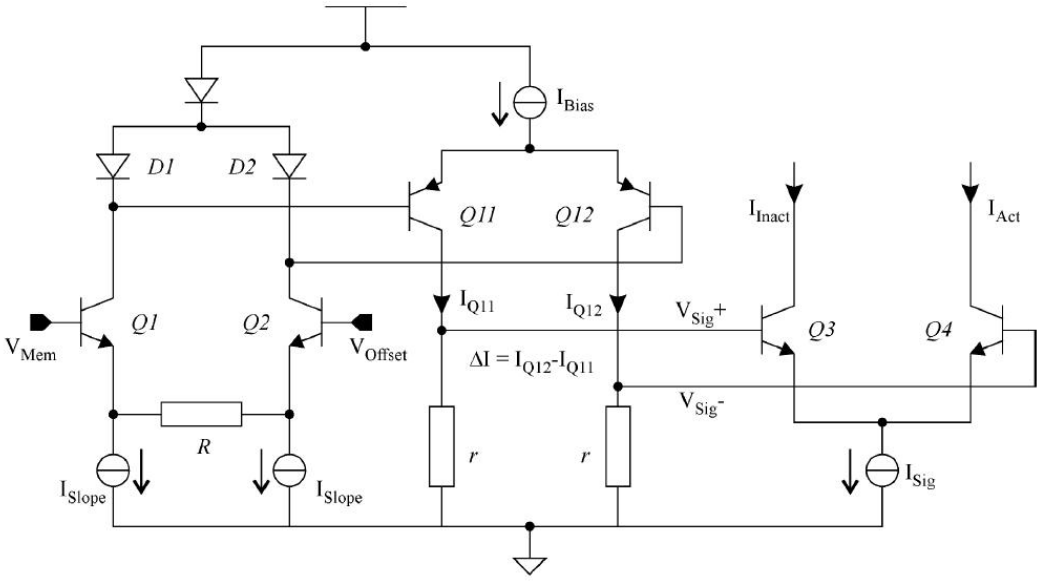

Figure 4.9: Tunable sigmoid function, with input voltage $V_{Mem} - V_{Offset}$ and output current I_{act} or I_{Inact} to compute the activation or the inactivation term, respectively [23].

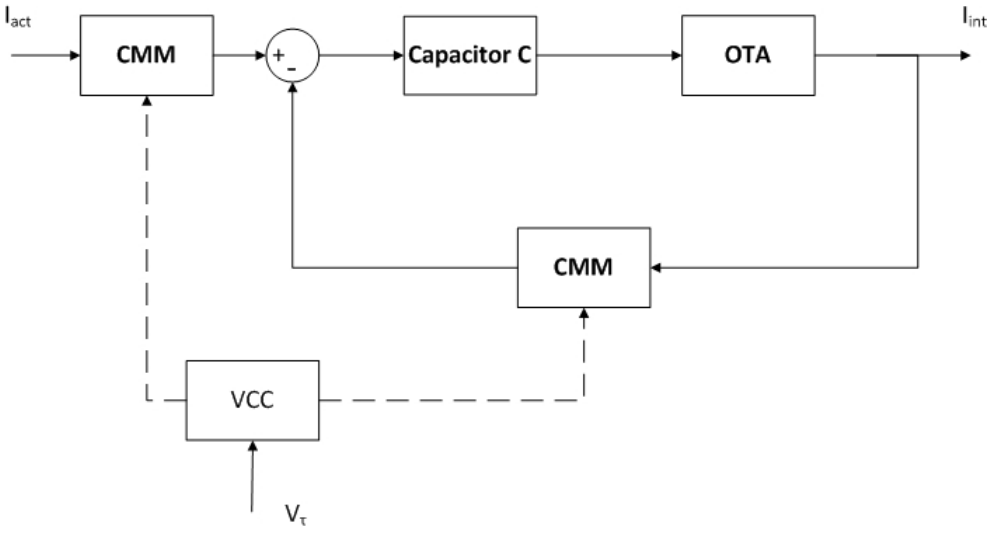

Figure 4.10: Circuit diagram of the integrator function. The input and output currents, respectively I_{act} and I_{inact}, are amplified by the current-mode multiplier (CMM). The second input to the CMM is current delivered by a voltage-controlled current (VCC) source, and the gain of the CMM is $A(V_\tau)$. The capacitor transfer function is $1/Cs$, and the gain of the OTA is B.

4.4.2 Kinetic function

The Kinetic function realizes a differential equation of the first order 1.4, where m_∞ is obtained by sigmoid function. To design this block we chose to use a closed loop integration

rather than a differentiator, for the noise immunity. The block diagram of Kinetic function is showed in Figure 4.10. From the block diagram we obtain the following equations:

$$\frac{C}{A(V_\tau) \cdot B} \cdot s \cdot I_{int} = I_{act} - I_{int} \tag{4.31}$$

where $\frac{C}{A(V_\tau) \cdot B}$ is the time constant, $A(V_\tau)$ is the gain of CMM and B is the gain of operational transconductance amplifier.

This structure contains two current-mode multipliers (CMM), to regulate the time constant τ for a voltage V_τ. Since the Kinetic input and output have the same algebraic sign and for simplicity reasons, we prefer to use a configuration with two one-quadrant multipliers rather than a single two-quadrant multiplier placed after a subtractor.

4.4.3 Power raising

This block multiplies and elevates to power the different terms of activation and inactivation, and to achieve it we use the same principle of CMM, namely the translinear loop principle. We have implemented all possible combinations exponentiation of p and q, according to the specification (i. e. mh, m^2h, m^3h and m^4). In the Figure 4.11, it is shown an example of power raising (m^3h). Applying the Kirchhoff's voltage law to the circuit in Figure 4.11, we obtain:

$$V_{BE_{Qh}} + V_{BE_{Qm}} + V_{D_{m1}} + V_{D_{m2}} - V_{BE_{Qout}} - V_{D2} - V_{D1} - V_{Q1} = 0 \tag{4.32}$$

Using transistors with the same surface we obtain:

$$I_{C_{Qh}} \cdot I_{C_{Qm}} \cdot I_{Dm1} \cdot I_{Dm2} = I_{C_{Qout}} \cdot I_{D2} \cdot I_{D1} \cdot I_{C_{Q1}} \tag{4.33}$$

Using the same approximation made for CMM namely whereas the collector current is equal to that of the emitter, we can write that $I_{C_{Qh}} = I_{Dm1} = I_{Dm2} = I_m$, $I_{C_{Qh}} = I_h$, $I_{C_{Q1}} = I_{D2} = I_{D1} = I_{Bias}$ and $I_{C_{Qout}} = I_{Power}$. Then considering this approximation, the equation (4.33) becomes:

$$I_{Power} = \frac{I_m^3 \cdot I_h}{I_{Bias}^3} \tag{4.34}$$

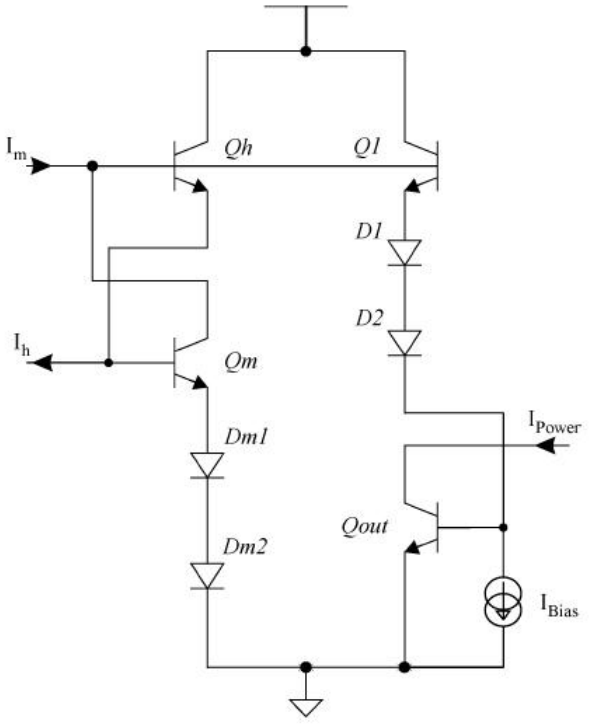

Figure 4.11: Circuit used for power raising, using the translinear loop principle. In that case, $I_{power} = I_m^3 \cdot I_h / I_{Bias}^3$[23].

4.4.4 Output multiplier

The last element of our library is the output multiplier, as shown in Figure 4.12. This stage consists of two mounting discussed earlier: the translinear loop principle and Operational Transconductance Amplifier. The bias current of the bipolar pair $Q_{11} - Q_{12}$ is replaced by $I_{Power} \cdot g_{Ion}$, where I_{power} is the output current of the power raising stage and g_{Ion} is the current generated by CMM. The collector current difference, between Q_{11} and Q_{12} , can thus be determined from equation (4.29). This collector current difference is afterwards multiplied by the ratio of the current mirror M_6 and M_8, that in this case it is 10. Then the output current is given by the following expression:

$$\Delta I = \frac{10}{R \cdot I_{Slope}} \cdot I_{Power} \cdot g_{Ion} \cdot (V_{Mem} - V_{Ion}) \tag{4.35}$$

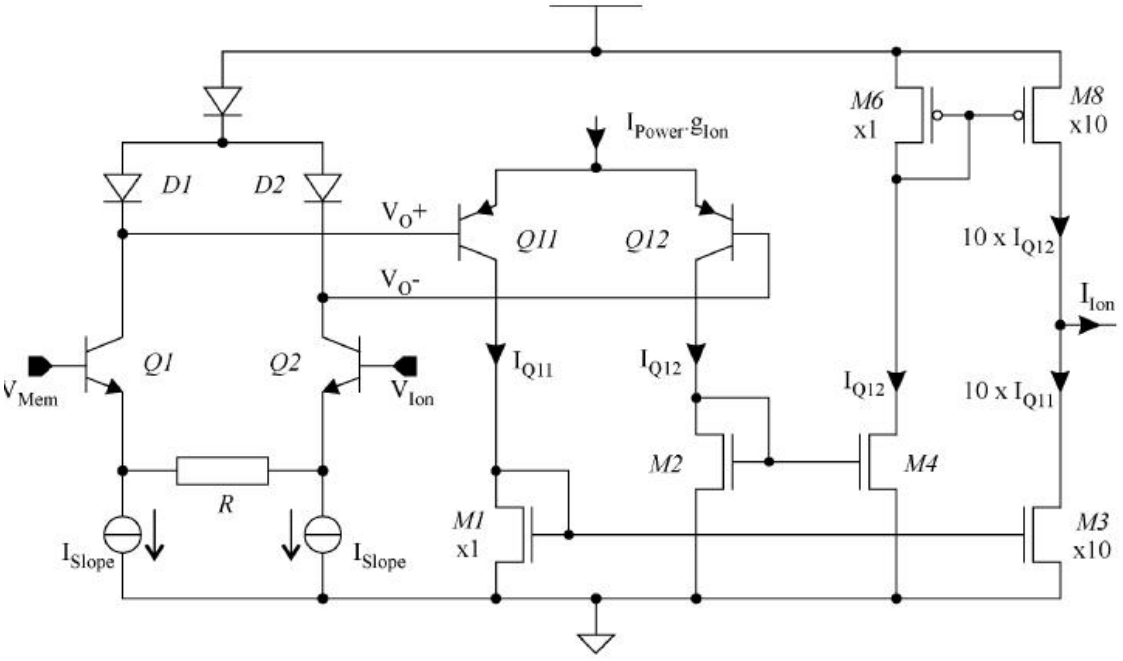

Figure 4.12: Multiplier circuit generating the ionic current I_{Ion}, with an input bipolar differential pair $Q_1 - Q_2$ controlled by V_{Mem} and V_{Ion} and a predistorsion stage $Q_{11} - Q_{12}$ biased by $I_{Power} \cdot g_{Ion}$ [23].

Chapter 5

Noise Implementation

In this chapter we explain the realization of a white noise with Gaussian distribution which will be added into variables gating of ion conductance according to equation 2.14. The white noise is produced by an analog random generator. The generator is composed by 64 cells, where each cell implements a switched-capacitor. The cells are connected as a MASH cascade in a ring topology. We start by introducing the basic cellular architecture, that is based by delta-sigma modulation and cascade structures. After we present its analog VLSI implementation. Finally, we explain the noise implementation into gating variable.

5.1 Noise generator

The easiest way to generate analog noise in VLSI is to amplify existing circuit noise, for example with such a high-gain comparator; for our application there exists a more powerful method to generate an uniformly distributed random analog value that controls the sensibility of the physical components and the uncorrelation between the cells neighboring is implemented in Analog VLSI random generator of Gert Cauwenberghs [24]. This approach uses noise-shaping properties observed in MASH cascade structures of delta-sigma modulators [25] as used for stable higher order oversampled A/D conversion [26] [27].

5.1.1 Sigma-delta modulation

The Sigma-delta modulation, that is the basic cell of the noise generator, uses a technique that effectively reduces the quantization error adding noise prior to the process of quantization, is called noise shaping. Noise shaping works by inserting the quantization error in a feedback loop. Any feedback loop works as a filter, so by creating a feedback loop for the

error itself, the error can be filtered as desired. Then, the output sample of noise shaping structure is equal to the input sample plus the quantization error on previous sample. Sigma-delta modulation uses oversampling and integration of the signal prior to quantization to increase the correlation between samples and decrease the quantization error. The main components of the first-order sigma-delta modulation are integrator, quantizer and feedback D/A converter as shown in Figure 5.1. Moreover, the MASH sigma-delta modulation through low-pass filtering allows to obtain the near-gaussian amplitude profile.

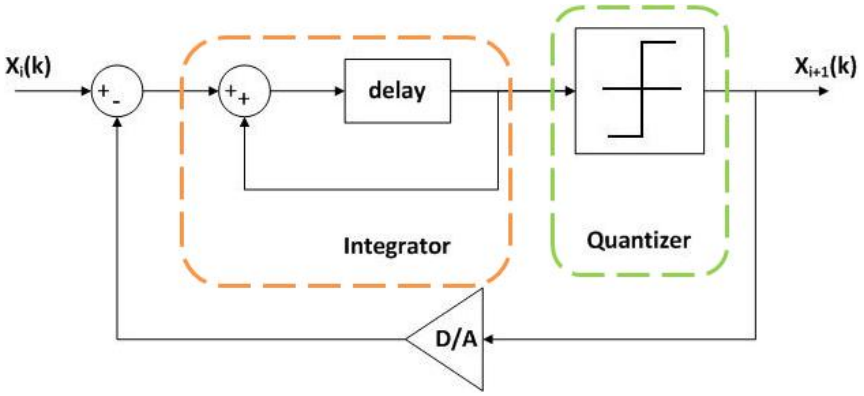

Figure 5.1: Block diagram of sigma-delta modulation.

The input-output characteristic, that you can call nonlinear map $f_{\Sigma\Delta}(\cdot)$, of such a sigma-delta modulator is plotted in Figure 5.2. It is analytically defined by

$$\begin{aligned} f_{\Sigma\Delta}(x) &= x - sign(x) \\ &= x - 1 \quad \text{if } x > 0 \\ &= x + 1 \quad \text{if } x \leq 0. \end{aligned} \tag{5.1}$$

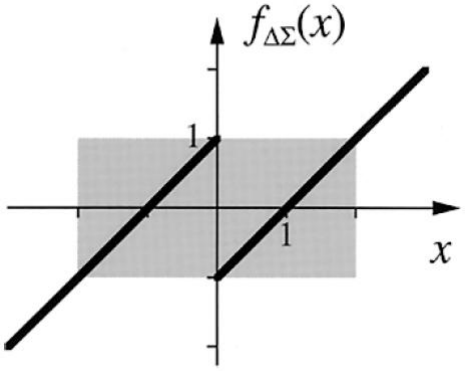

Figure 5.2: The nonlinear map $f_{\Delta\Sigma}$ of single delta-sigma modulation [26].

5.1.2 Cellular structure

If you connect the sigma-delta modulation, their interactions are defined as

$$x_i(k+1) = f_{\Sigma\Delta}\left(\alpha + \beta \sum_{j \in N(i)} x_j(k)\right) \tag{5.2}$$

Where $N(i)$ defines a neighborsorhood of cells interacting with cell i including itself, and $f_{\Sigma\Delta}(\cdot)$ is a sigma-delta nonlinear maps that is defined of equation 5.1. The constants α and β have a value critical to the randomness properties of the sequence $x_i(k)$.

The form that expresses the general nearest-neighbor interaction, in equation (5.2), can

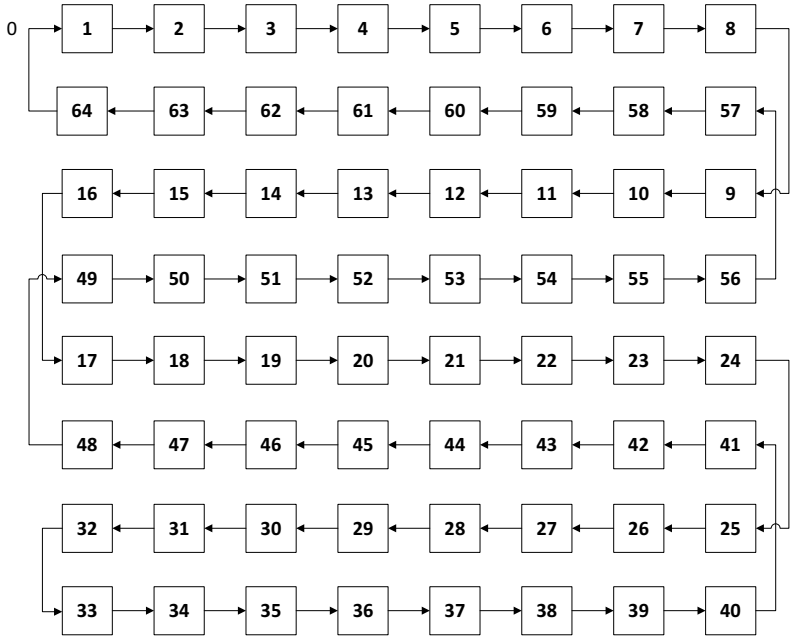

Figure 5.3: Array of 64 MASH random generating cells. Linear cascaded ring topology implemented on a 2-D grid.

describe cellular networks of various topologies. The simplest case is considered a network formed by two neighboring cells. With $\alpha = 0$ and $\beta = 1$ we obtain:

$$x_i(k+1) = f_{\Sigma\Delta}\left(x_i(k) + x_{i-i}(k)\right) \tag{5.3}$$

This describes the behaviour of a MASH cascade. The MASH cascade consist of multi-connected single integration delta-sigma modulation loops. A possible implementation of this cascade structure of N cell is a ring. In the ring topology the last cell of the chain is connected to the first cell.

The linear cascaded ring topologies can be implemented in scalable cellular VLSI architectures on 2-D grid shown in Figure 5.3, it is realized by two sets of linear cascade segments interleaved in opposing directions. The ring structure on 2-D grid is preferable because of symmetry which provides more uniform random noise properties across the array and it presents a compact analog VLSI implementation. The independence of the output signal of the cell $x_i(k)$ with the output signal of the cell $x_{i+1}(k)$, of a MASH cascade structure is established by Theorem [24]:

Theorem 5.1.1. *The vector sequence* $x_i(k),\ i = 1\cdots N,\ k = 1\cdots\infty$ *obtained from a cascade of modulators according to equation (5.3) with initial conditions* $-1 \leq x_i(0) \leq 1$ *and boundary conditions* $x_0(k)$ *drawn from an uniform random distribution, i.e.:* $p^{k,l}_{0,0}(x|y) \equiv p^k_0(x) = 1/2, \forall\ x, y \in [-1, 1]; k \neq l$*, allows an uniform random distribution with mutually statistically independent components, i.e.:* $p^{k,l}_{i,j}(x|y) \equiv p^k_0(x) = 1/2, \forall\ x, y \in [-1, 1]$*; where either* $k \neq l$ *or* $i \neq j$

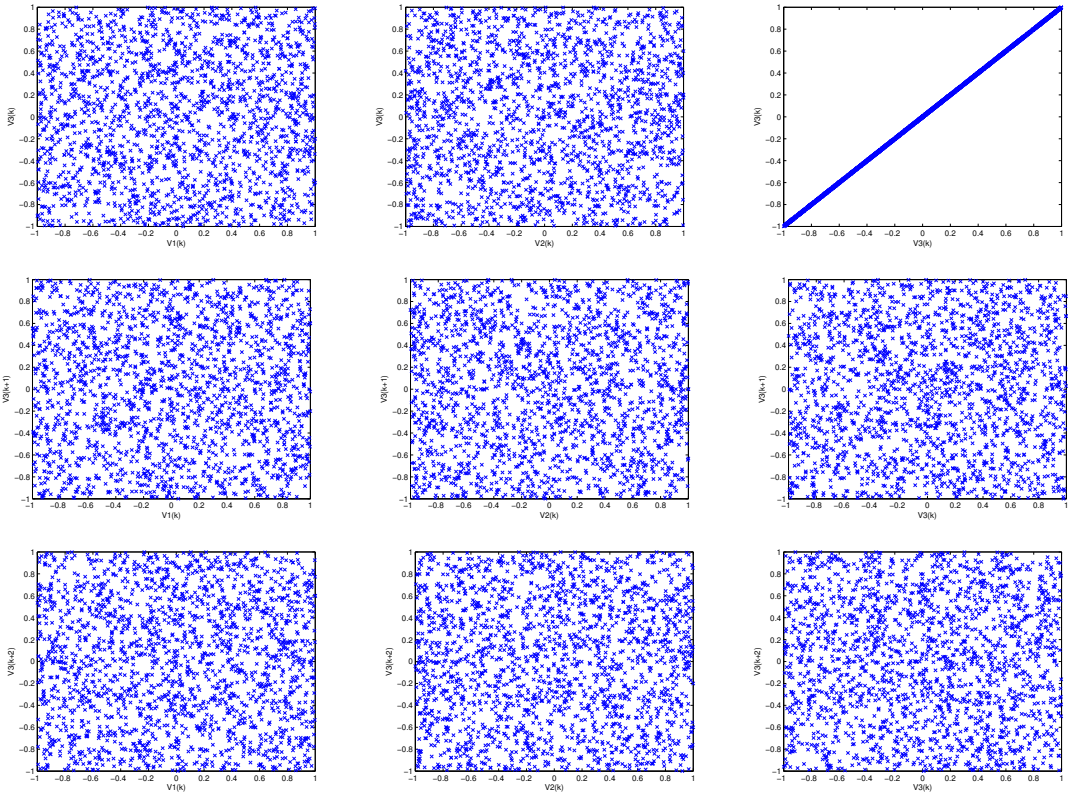

Figure 5.4: MATLAB simulation of time-spice correlogram. Scatter plots of data from the 64-cell ring, across three neighboring cells and three consecutive time delays.

This theorem allows to say that when we impose an uniform random input to the first

element in a MASH cascade, all cells produce an uncorrelated uniform random outputs, as represented by Figure 5.4.

5.2 Noise generator implementation

The basic delta-sigma modulation cell is implemented for the switched-capacitor architecture, that realizes the function of integration and quantizer, with a one-bit D/A converter is shown in Figure 5.5.

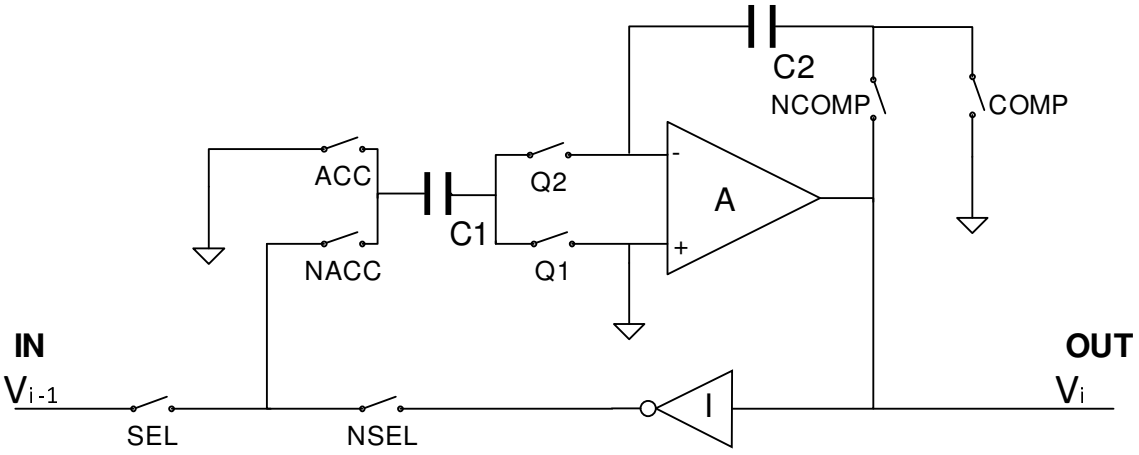

Figure 5.5: Switched-capacitor MASH modulator cell.

5.2.1 Switched capacitor integrator

The main element of this structure is a switched capacitor integrator. The switched-capacitor integrator uses switches, operational amplifiers and capacity, to realize the function of integration. This idea has been developed to allow the analog and digital integration on a chip. In fact, we use for this structure the basic elements of a VLSI integration as the MOS transistors, and the capacitors. The basic principle of this technique is the replacement of a resistor and a switched capacitor, as shown in Figure 5.6.
Given, 2 non-overlapped clocks (Q_1 to Q_2), each of frequency f = 1/T, the structure consists of 2 switches and the capacity is equivalent to a resistance inversely proportional to the value of the capacitor and the frequency of the following phases:

- Q_1 active, across the capacitor C_1 a voltage V1 is applied and then has a charge equal to $Q_C = C_1 \cdot V_1$;

- Q_2 active, across the capacitor C_1 a voltage V2 is applied and then has a charge equal to $Q_C = C_1 \cdot V_2$.

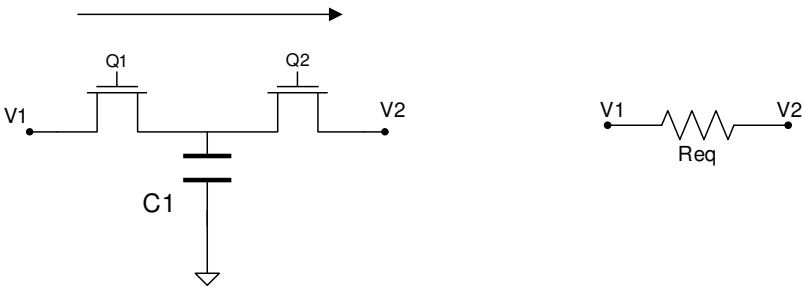

Figure 5.6: Principle switched capacitor.

The average current is then given of the charge divided by the time (T) in which charge is transferred from V1 to V2 during τ:

$$\Delta Q_C = C(V_1 - V_2)\tau \tag{5.4}$$

The quantity of charge transferred between across the resistor V1 and V2 during τ is

$$\Delta Q'_C = \frac{(V_1 - V_2)}{R}\tau \tag{5.5}$$

The conditions under which the two transfers $\Delta Q'_C = \Delta Q_C$ are the same is the following:

$$R = \frac{T}{C} = \frac{1}{C \cdot f} \tag{5.6}$$

If we create a low-pass filter, for example, with this methodology, its parameters do not depend on absolute values of capacity and resistance but depend on the ratio between two capacitors that can be made very precise. This allows to create filters that would be impossible with only resistors and capacitors because requirements will be too high (impossible on a single chip).

Normally, the capacitors used are those made with two plates stacked polysilicon (capacity poly-poly2). In addition to the desired capacitor (C_1), these structures introduce two parasitic capacity (C_{p1} and C_{p2}) of which especially that associated with the bottom plate can be very large, about 5 to 20% of capacitor C_1 realized. The circuits based on these capacitors must take account of these parasites devices.

To eliminate the parasitic capacity, between the possible configurations of switched-capacitors integrator, we use the configuration in Figure 5.7. This configuration is insensitive to parasitic capacity because they are eliminated: C_{p4} does not count because it is

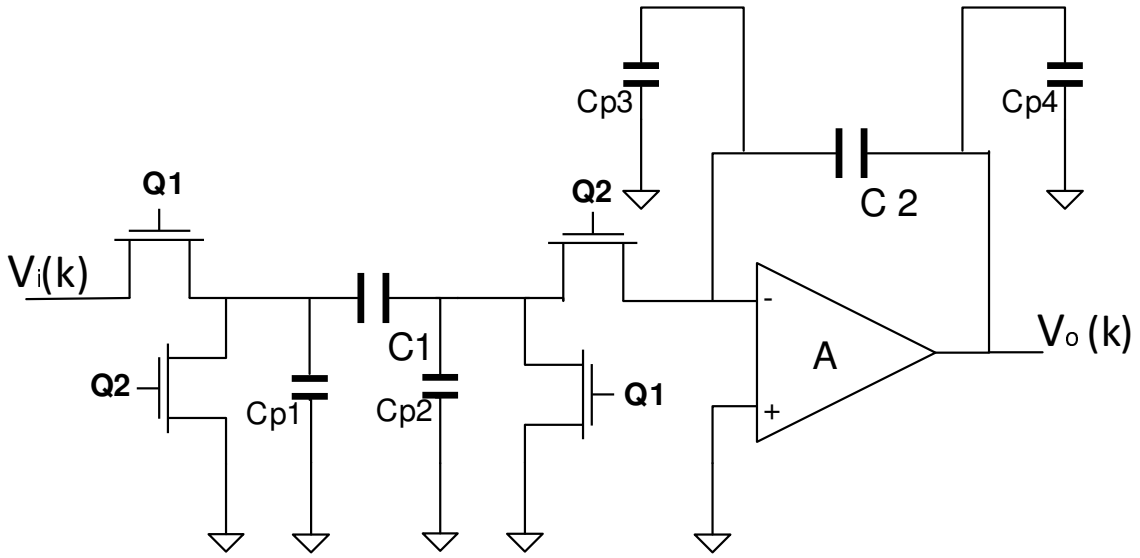

Figure 5.7: Switched capacitor integrator insensitive to parasitic capacity.

an output. C_{p3} is shorted (via the virtual mass). C_{p2} is shorted in both Q_1 (via switch) is in Q_2 (via virtual mass). C_{p1} has no effect because it is in parallel with C_1 and this only when connected to the input, but when Q_2 is high, C_{p1} is discharged by the switch and does not affect the charge stored on C_1 is therefore unaffected.

5.2.2 Behaviour of sigma-delta modulation

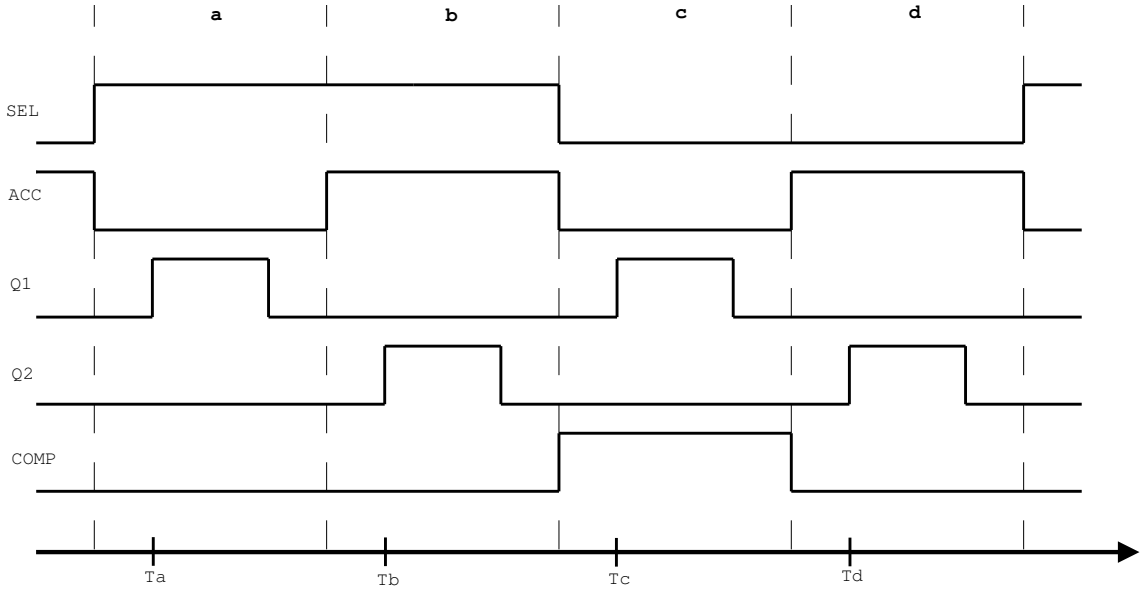

Figure 5.8: Timing diagram of Switched-capacitor MASH modulator.

The Sigma-delta modulation is composed by four phases, which are shown in Figure

5.8. We can see that during the process of the switched-capacitor non inverting integrator (controlled by signals Q1, Q2, ACC) phases a-b and c-d are the same. If SEL is high the value stored across capacitor C_1 is $V_{i-1(k)}$ (input voltage), while, if SEL is low, the value stored across capacitor C_1 will be the output voltage of the comparator inverted of the one-bit D/A converter I. When the COMP signal is high, the amplifier A operates as a comparator: it compares V_i to zero and it presents the result (V_i's sign) to the accumulator's input by inverting of one-bit the D/A converter. The amplifier works as an accumulator 1/(1-z) and a quantizer $f_{\Delta\Sigma}$. On the other hand, when the COMP signal is low, $V_i(k)$ is presented in output.

Following the charge conservation principle, the analysis of the sigma-delta modulation develops in the following 4 phases (Figure 5.9):

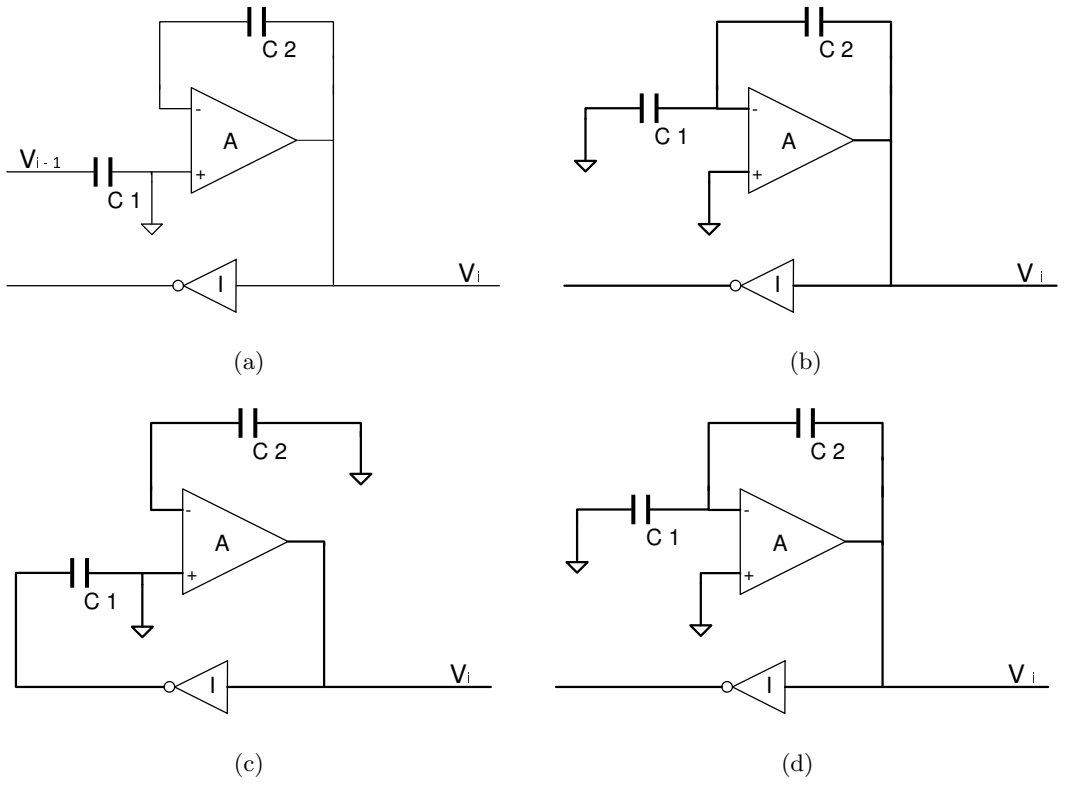

Figure 5.9: Simplified diagram of the 4 phases of operation of Switched-capacitor MASH modulator.

- **Phase a** (instant Ta): the voltage across C_1 is equal to the input voltage and the voltage across C_2 is equal to the previous output voltage:

$$V_{i-1}(k + Ta) = -V_{C1}(k + Ta) \tag{5.7}$$

$$V_i(k+Ta) = V_{C_2}(k+Td) \tag{5.8}$$

Then the charges on the two capacitors will be:

$$Q_{C_1}(k-Ta) = -C_1 V_{i-1}(k-Ta) \tag{5.9}$$

$$Q_{C_2}(k-Ta) = C_2 V_i(k-Td) \tag{5.10}$$

- **Phase b** (instant Tb): at the heads of C_1 there is no voltage, then the charge Q_1 must leave C_1 moving to C_2:

$$Q_{c1}(k-Tb) = 0 \tag{5.11}$$

$$Q_{c2}(k-Tb) = Q_{c2}(k-Ta) - Q_{c1}(k-Ta) = C_2 V_i(k-Ta) + C_1 V_{i-1}(k-Ta) \tag{5.12}$$

$$V_i(k-Tb) = Q_{c2}(k-Tb)/C_2 = V_i(k-Ta) + C_1/C_2 V_{i-1}(k-Ta) \tag{5.13}$$

this phase produces $X_i(x) + X_{i-1}(k)$.

- **Phase c** (instant Tc): the amplifier A compares the C_2's voltage with zero, the result is inverted and stored in C_1:

$$V_i(k-Tc) = A(V_{c2}(k-Tb) - 0) \tag{5.14}$$

$$V_{inverter}(k-Tc) = \pm 1V \tag{5.15}$$

Then the charges on the two capacitors will be:

$$Q_{c2}(k-Tc) = Q_{c2}(k-Tb) \tag{5.16}$$

$$Q_{c1}(k-Tc) = -C_1 V_{inverter}(k-Tc) \tag{5.17}$$

- **Phase d** (instant Td): at the heads of C_1 there is no voltage, then the charge Q_1 must leave C_1 moving to C_2 and the $V_i(k+1)$ accumulates in C_2:

$$Q_{c1}(k-Td) = 0 \tag{5.18}$$

$$Q_{c2}(k-Td) = Q_{c2}(k-Tc) - Q_{c1}(k-Tc) = C_2 V_i(k-Tc) + C_1 V_{inverter}(k-Tc) \quad (5.19)$$

$$V_i(k-b) = Q_{c2}(k-d)/C_2 = V_i(k-c) + C_1/C_2 V_{inverter}(k-c) \quad (5.20)$$

during this phase accumulate substrats the sign of the accumulate in phase b, obtaining $f_{\Delta\Sigma}(X_i(x) + X_{i-1}(k))$.

5.2.3 CMOS implementation

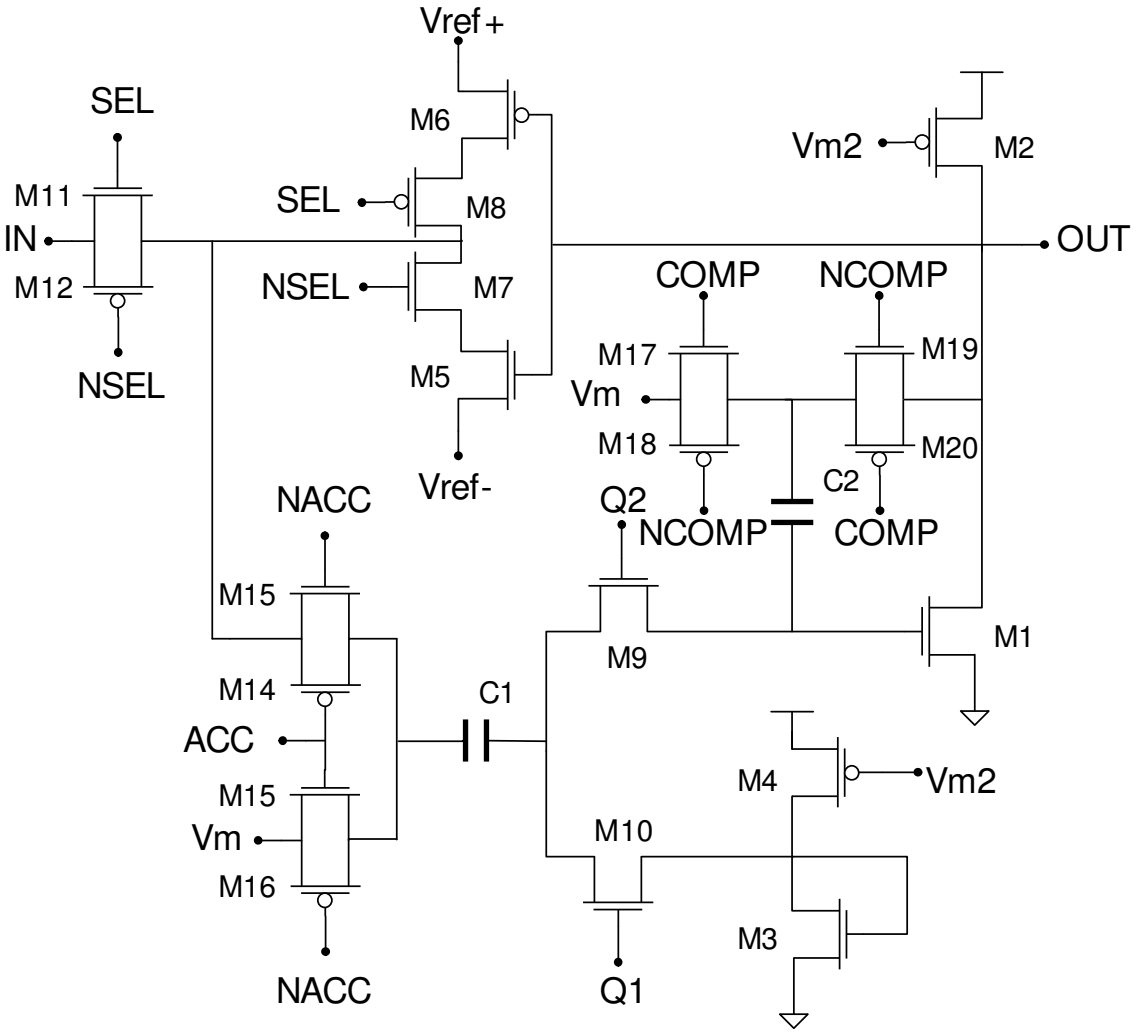

Figure 5.10: CMOS switched-capacitor circuit diagram of MASH modulator cell (MASC-cell).

The noise generator is composed of 64 MASH Cell, Figure 5.10 shows the transistor-level circuit of the single MASH cell. For low-power consumption we chose a single power

supply to 3V. In the resource of neurons implemented in this chip, the action potential period is about 0.02 ms. We use a clock at 400KHz to introduce a number of significant fluctuations during the action potential. However, the clock signal can be changed because it is driven from the outside by a FPGA.

The Vm, signal ground level, is fixed to 1.5V and the the D/A levels are V_{ref-}=0.9 V and V_{ref+}=2.1V thus the signal range is $\pm 0.6V$ by V_m. The two capacitances, C_1 and C_2 are 1pF, that corresponds to 3 capacitors of C_{min} of 0,333pF in BiCMOS 0.35 um SiGe. The value of two capacitor is the same because DC gain of switched capacitor integrator takes the value of one. The amplifier A is implemented as simple common source N-MOS of M1-M2 transistor, were chosen the size of the transistors (W_1/L_1 and W_2/L_2) in order to have a $A_v = 20dB$. The virtual ground voltage of the amplifier is obtained from circuit M3-M4, in which the V_{m2} is the bias voltage.

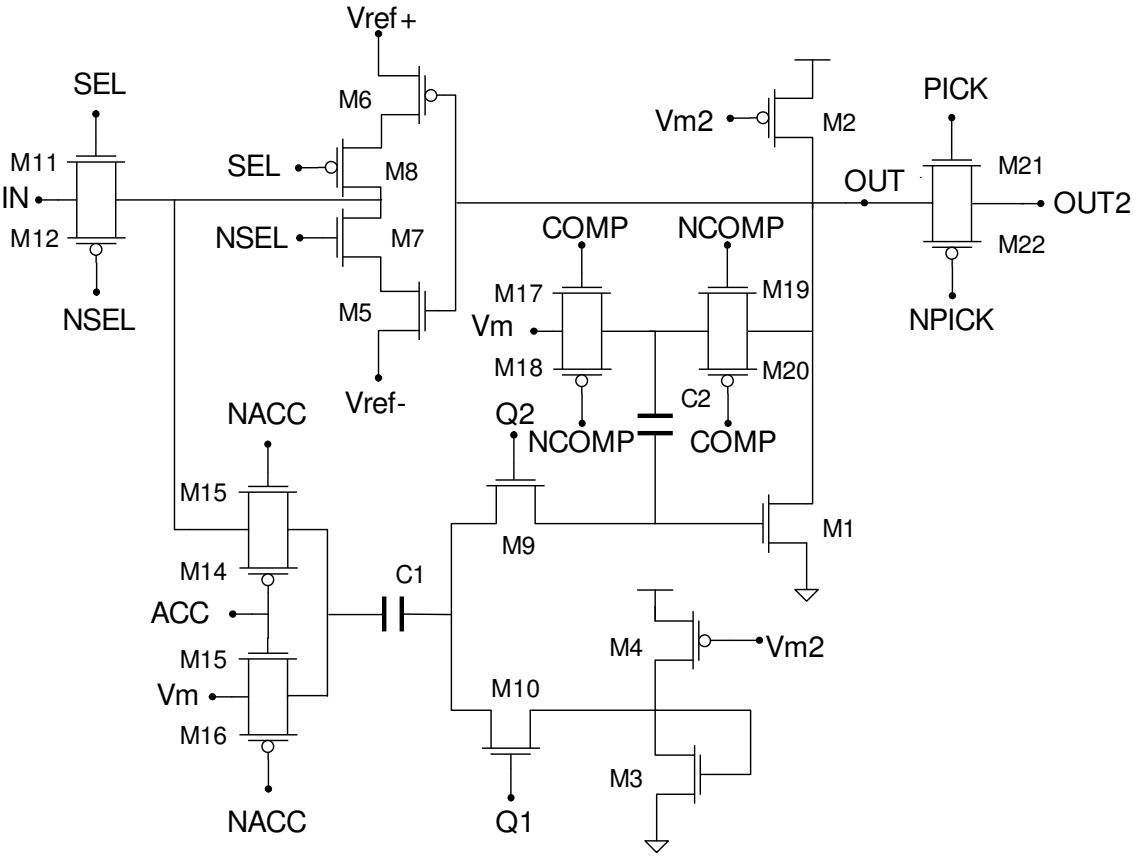

Figure 5.11: CMOS switched-capacitor circuit diagram of MASH modulator cell with an additional output out_2 (MASCcell2).

In the sigma-delta modulation the switches are formed by the parallel of two transistors N-MOS and P-MOS so that the output switches from Vdd to 0 regardless of the input

value. The size of the transistors in the switches is chosen as small as possible in order to have high speed switchings.

From the simulations we have seen that in order to maintain the status value of the output of the sigma-delta modulation obtained from phase d for the four phase subsequent we have to add a switch in the output as in Figure 5.11. This switch is controlled by a clock signal PICK that actives for a short time in phase d and the output signal remains constant. In Figure 5.12 is shown the new timing diagrams.

To optimize the layout we create two different cells: one with a similar structure to that

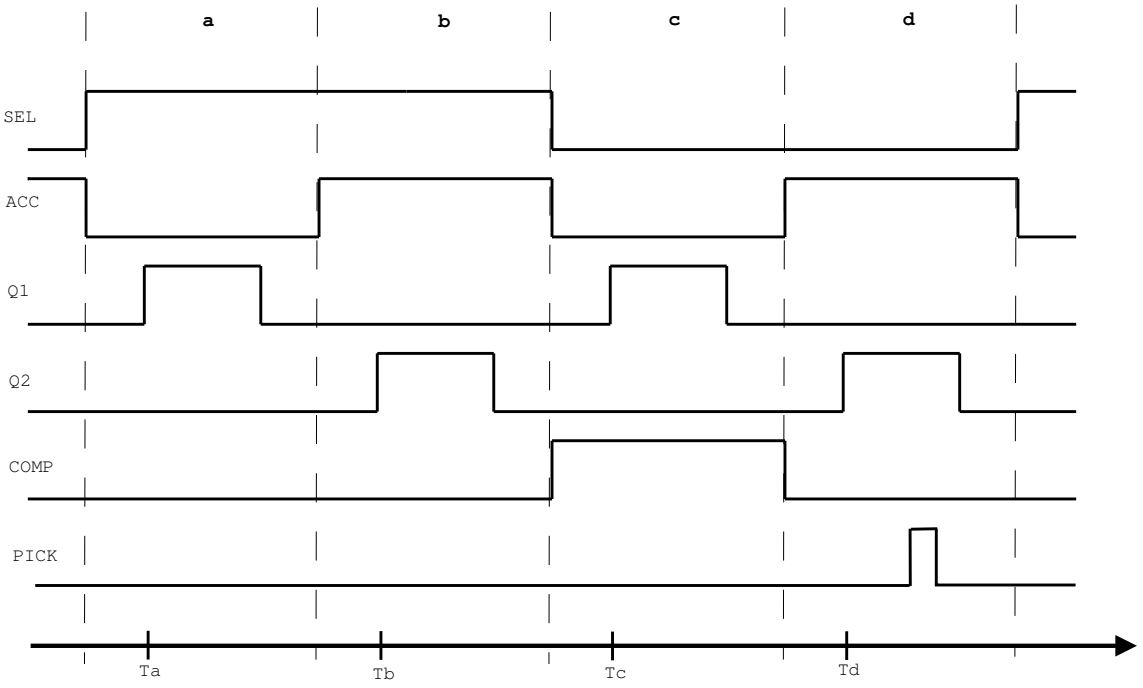

Figure 5.12: Timing diagram of Switched-capacitor MASH modulator with an additional output out_2.

of the sigma-delta modulation, which we call MASCcell. The second cell is equal to that of the sigma-delta modulation adding a switch in output out that we call MASCcell2. The output out of the cell MASCcell2 is connected to the next cell and the output out2 is the output of noise generator. Our CPR network consists of two CPR neurons and of four FS neurons. If we consider the conductances of all neurons, five for CPR neuron and three for FS neuron we get twenty two conductance where we add the noise. Given the uncorrelation between the outputs of noise generator, we generate the twenty-two signals with a single generator, and we take twenty-two outputs from MASCcell2. The noise generator is essentially composed of 2 cells that are repeated, then we used semi-custom

design. To realize the layout of the generator we follow 2 steps: the first we create the main 2 cells, by placing the polarization signals on the top, the clock signals at the bottom, the input at the right and the output at the left of the cell.
Then we place the 2 cells in a matrix eight rows and eight columns, as shown in Figure 5.3, to obtain the particular 2-D structure of the noise generator, and a higher integration density. All the cells in the odd rows are inverted (in Figure 5.13 the cells inverted have a star) so that the cell lines have in common the pins with the row above and the one below. The twenty-two outputs of MASCcell2 together with an output of MASCcell test are positioned on the left.

Transistor	W(um)	L(um)
M_1 and M_2	20	1
M_3 to M_8 and M_{11} to M_{22}	6	1
M_9 to M_{10}	3	1

Table 5.1: Summary table of the size of transistors, in the sigma-delta modulation, used in MASCcell and MASCcell2.

Bias tension	(V)
V_m	1.5
V_{m2}	0.6
V_{ref+}	2.1
V_{ref-}	0.9

Table 5.2: Bias tension

Clock signal	Voltage (V)	Delay time (us)	Rise time (ns)	Fall time (ns)
Q_1	0-3	0,4	50	50
Q_2	0-3	1.65	50	50
$COMP$	0-3	2,8	50	50
ACC	0-3	0,3	50	50
SEL	0-3	0,3	50	50
$PICK$	0-3	4800	50	50

Clock signal	Pulse width (ns)	Period (us)
Q_1	950	2.5
Q_2	950	2.5
$COMP$	1200	5
ACC	1200	2.5
SEL	2.45	5
$PICK$	0.3	5

Table 5.3: Clock signal

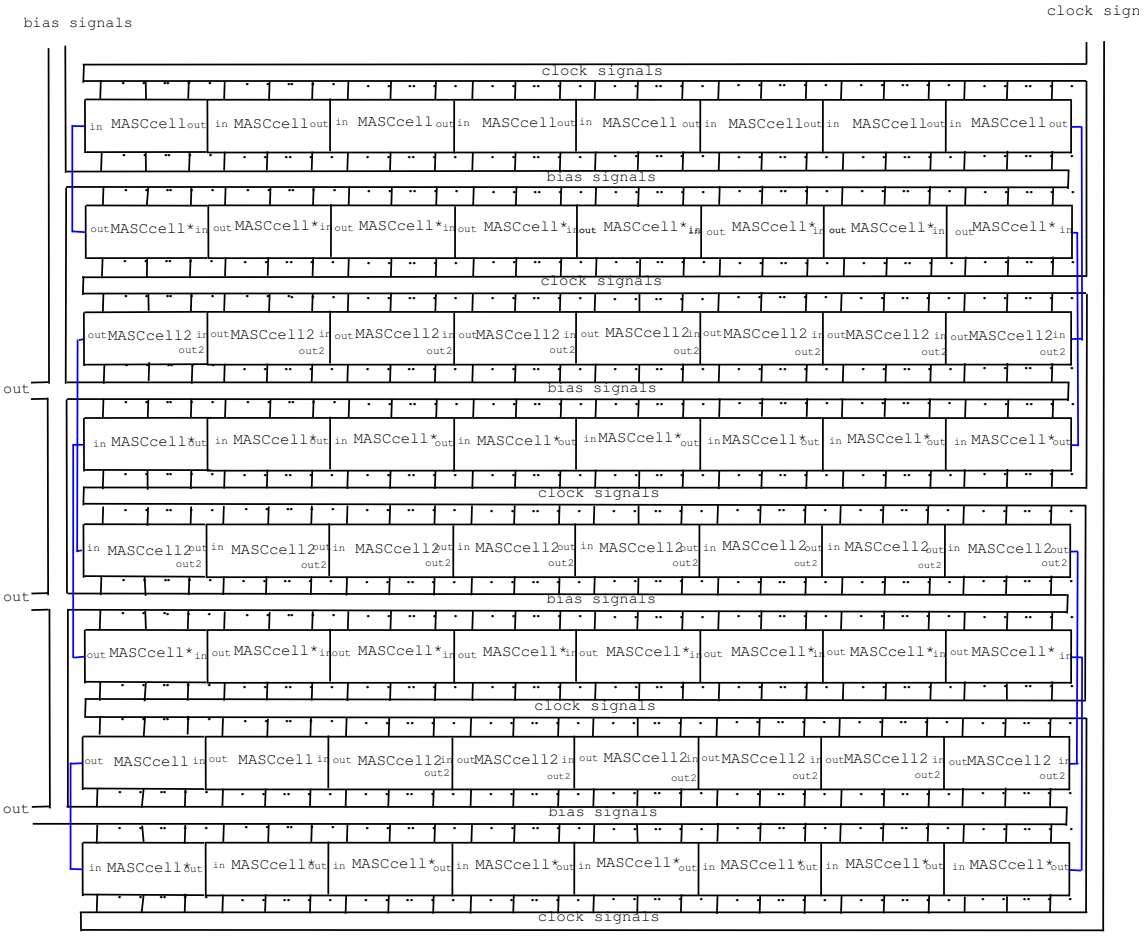

Figure 5.13: Layout diagram of Array of 64 MASH random generating cells.

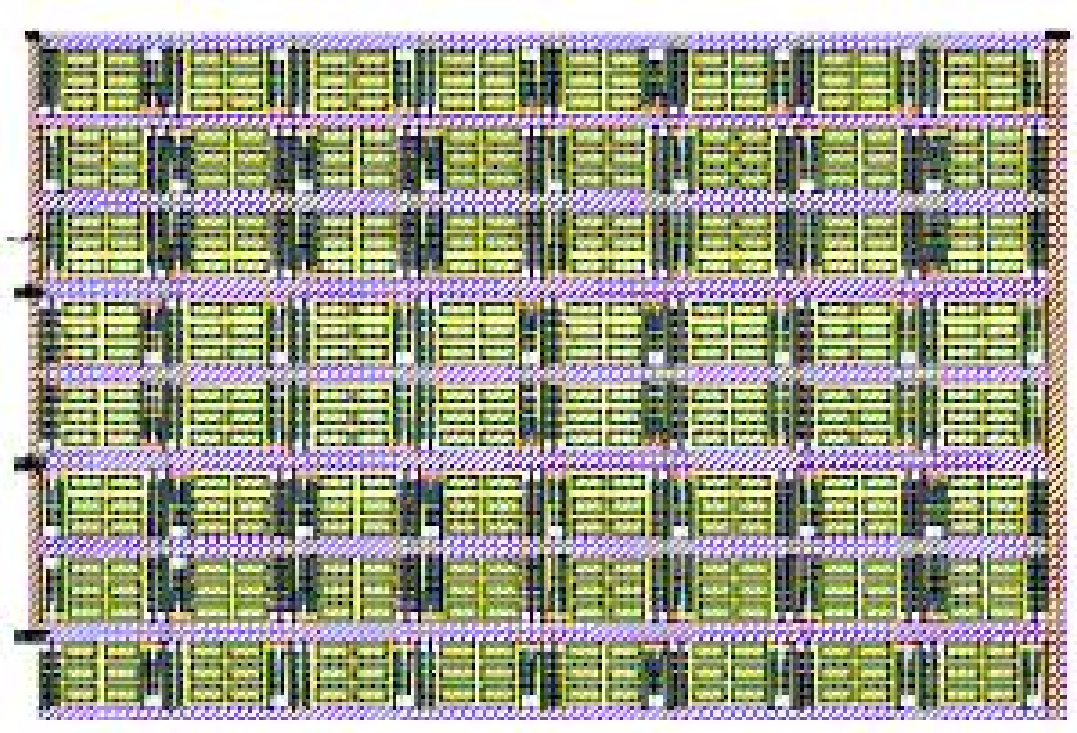

Figure 5.14: Layout of Array of 64 MASH random generating cells.

5.3 Results

We present the result of the simulation in Cadence of the noise generator of 800us. Figure 5.15 shows the trends of first three outputs of MASCcell2. We can observe that the circuit needs about 10 cycles (which is about $50us$) and the signal is confined between V_{ref+} and V_{ref-}. The statistical independence' s hypothesis is verified by Figure 5.16 with same method used in the MATLAB simulation represented by Figure 5.5. For this simulation we did not consider the sample of initialization time.

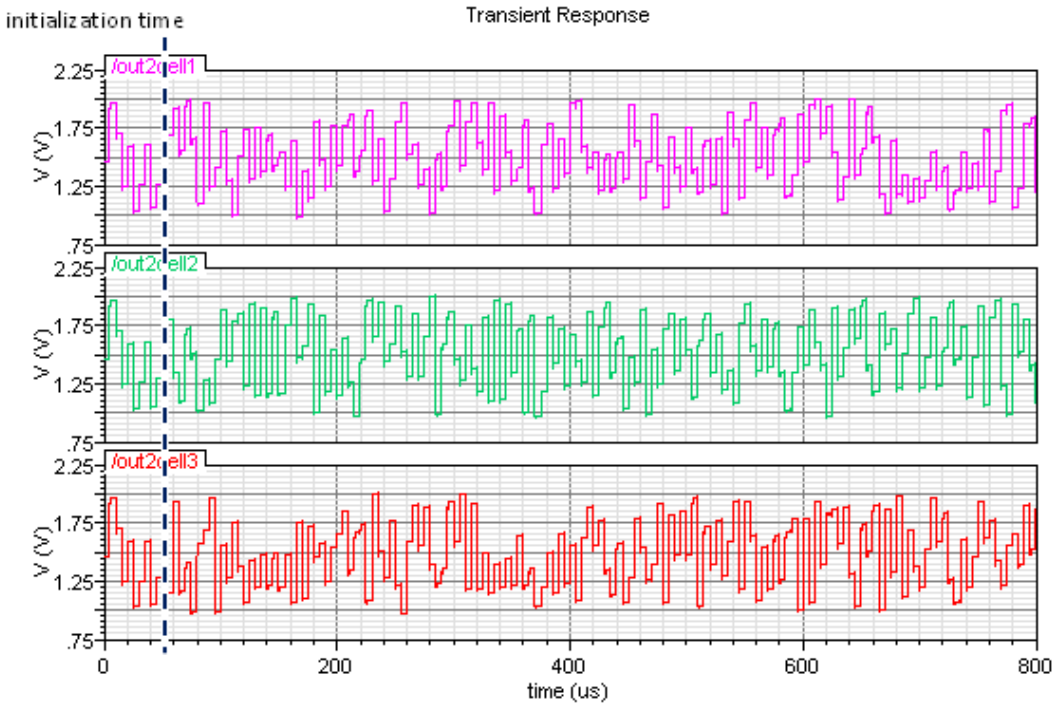

Figure 5.15: Cadence simulation of the first three cells of Array of 64 MASH random generating: out2cell1, out2cell2 out2cell3 are the outputs of MASCcell2

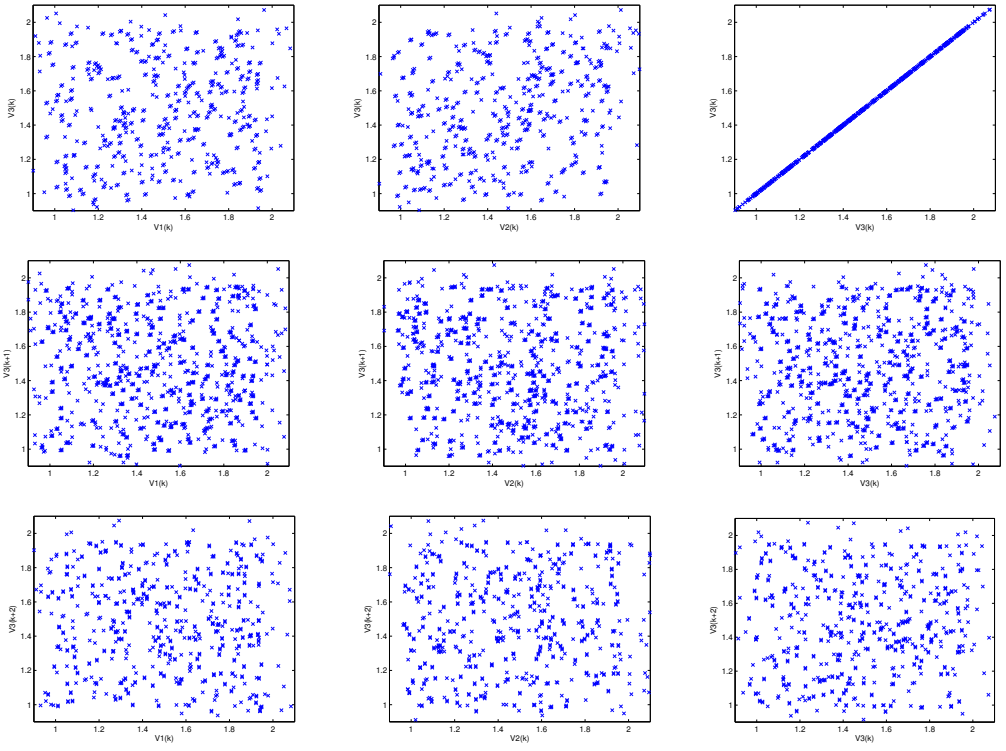

Figure 5.16: CADENCE simulation of time-spice correlogram. Scatter plots of data from the 64-cell ring, across three neighboring cells and three consecutive time delays.

5.4 Noise implementation into gating variables

In Chapter 2 we saw that in order to obtain a stochastic neuron, we must add a Gaussian white noise in the variables of activation or inactivation (gating variable) according to the equation (2.13). Then the equation of the kinetic function (4.31) becomes:

$$\frac{C \cdot s}{A(V_\tau) \cdot B} I_{Int} = I_{Act} - I_{Int} + I_{noise} \tag{5.21}$$

where I_{noise} is the noise current. In Figure 5.17 we show the new block diagram of Kinetic faction. To implement equation (5.21) we need a current I_{noise}, but the output of the

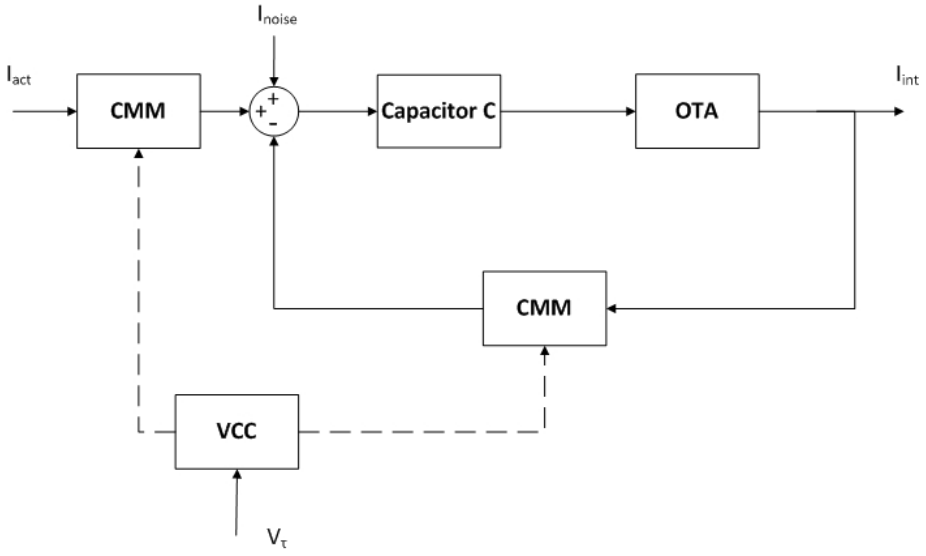

Figure 5.17: Block diagram of Kinetic faction with noise

noise generator we have a voltage, therefore we must make a current-voltage conversion. According to these considerations, we can define the block diagram of stochastic ionic current generators as shown in Figure 5.18.

The current-voltage conversion is realized by MOS Operational Transconductance Amplifier as shown in Figure 4.7. The differential pair of $M_1 - M_2$ is simply used to convert the noise voltage into the noise current, then the gate of M_1 is applied the voltage out2 and to the gate of M_2 is applied to the voltage V_m, that is the reference to the virtual mass of the noise generator. Another very important aspect of the converter is that it controls the noise amplitude. This is done by controlling the biasing current (I_{Bias}) for the differential pair that converts noise voltage into the noise current. As we saw in Chapter 2, in particular in the equation (2.14) the amplitude of the noise varies for each conductance, and then to determine the value of the amplitude of the voltage clamp, we use the method to

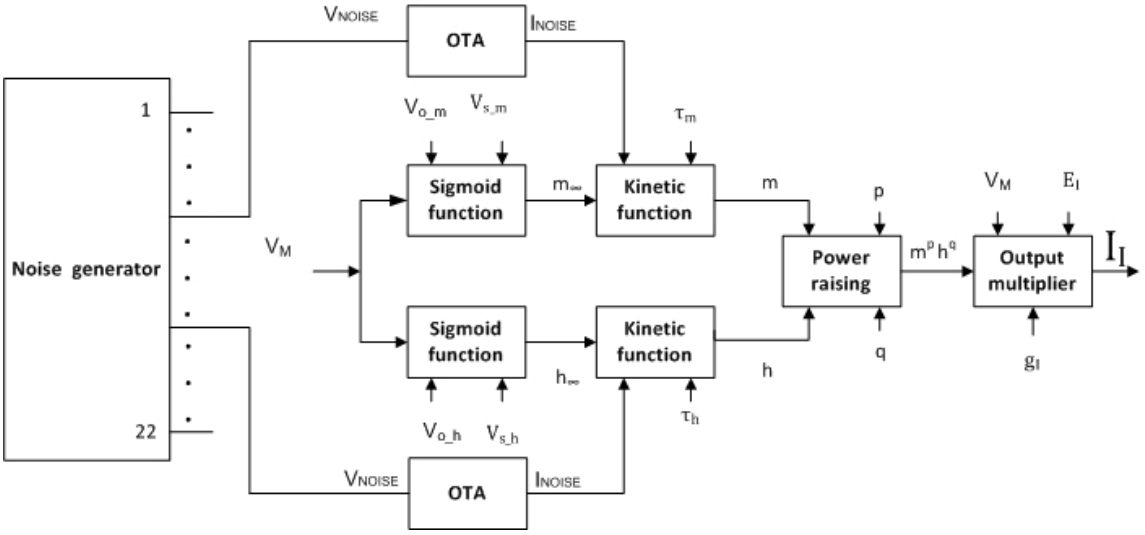

Figure 5.18: Block diagram of stochastic ionic current generators

analyze the contribution of the noise in the Kinetic function.

The voltage clamp is used by electrophysiologists to measure the ion currents across the membrane of excitable cells, such as neurons, while holding the membrane voltage at a set level. The voltage clamp allows to impose a tension in the membrane voltage and measure the corresponding ionic currents generated by neuron. In MATLAB we simulated the technique of voltage clamp of a FS neuron according to the equation (2.14), using a $\sigma = 0.02$ and imposing a tension membrane shown in Figure 5.20. In Figure 5.19 are represented gating variable obtained with this method.

We apply this method to the conductance implemented in Cadence. From simulations we obtain, for example, for the variable activation of sodium m a variation between 0 and 20uA then we must multiply the amplitude of the noise obtained in MATLAB for 20uA so the noise will have to have an amplitude of 4uA and then the current polarization that we must impose on the MOS Operational Transconductance Amplifier will be of $\pm 0.2uA$. This process is applied to all the gating variables of the HN, IN and CPR neurons. In table 5.4 are summarized noise parameters for designing the conversion voltage current to be added in the Kinetic block for each gating variable.

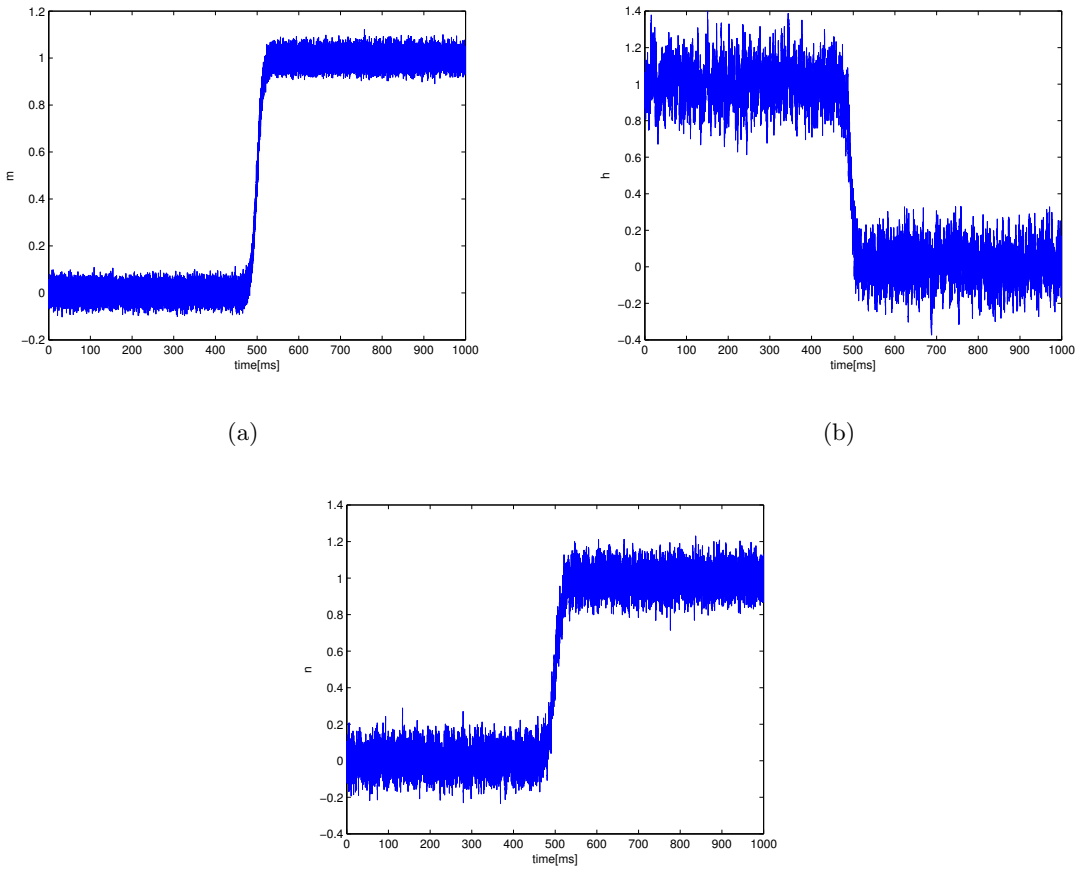

(a) (b)

(c)

Figure 5.19: MATLAB simulation of gating variables with voltage clamp method: m(a), h(b) and n(c).

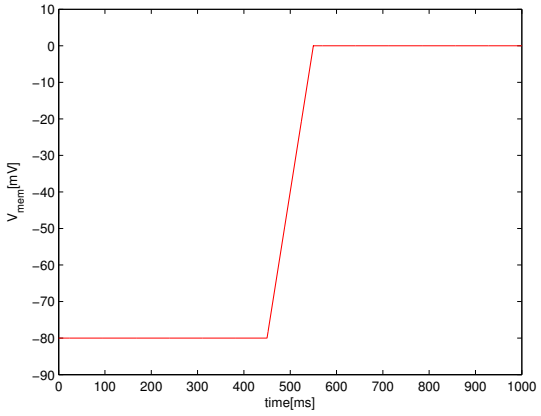

Figure 5.20: Behaviour of the membrane voltage imposed for the voltage clamp.

neuron type	**ion current**	σ	**gating kinetics**	**amplitude noise in gating kinetics**	**amplitude noise current**
HN	I_{Na}	0.02	m	± 0.1	$\pm 0.2uA$
		0.02	h	± 0.4	$\pm 0.8uA$
	I_K	0.02	n	± 0.2	$\pm 0.4uA$
IN	I_{Na}	0.02	m	± 0.1	$\pm 0.2uA$
		0.02	h	± 0.4	$\pm 0.8uA$
	I_K	0.02	n	± 0.2	$\pm 0.4uA$
CPR	I_{Na}	0.02	m	± 0.1	$\pm 0.2uA$
		0.02	h	± 0.4	$\pm 0.8uA$
	I_K	0.02	n	± 0.2	$\pm 0.4uA$
	I_{slowK}	0.02	o	none	none
	I_{slowNa}	0.02	s	none	none

Table 5.4: Noise parameters

Chapter 6

Conclusion

Noise in neural network is an important issue to understand the phenomena of learning, synchronization in network and eventually some kind of neural diseases. In this thesis we focus on the design of stochastic hardware neural network which will be connected to biological neural network thanks to the hybrid (artificial-biological) technique. The collaboration of my team with the National Tsing Hua University in Taiwan allows us to develop this hybrid technique with crayfish stomatogastric network.

The CPR network is a neuronal network consisting of 6 neurons and 12 synapses. Some interesting electrophysiological phenomena are modelled and mainly attributed to the interactions between the two kinds of sensory neurons in this network, i.e, the CPR neuron and the hair neuron. These phenomena have been rebuilt in Matlab and VerilogA simulation. The CPR neurons in the crayfish can be modelled as a FS neuron with two additional ion channels. One injects currents slowly to the membrane and the other one with a larger time constant leaks current slowly out of the membrane.

We presented in this thesis the Hodgkin-Huxley formalism that is a conductance based model of neurons. We proposed the stochastic neuron model which adds noise into the gating variables of ion conductances. We also verified that our new stochastic neuron model actually succeeds in reproducing the biological neural behaviour. In chapter 4, we present the library of analog operators based on the Hodgkin-Huxley Formalism to achieve the HN, IN and CPR neurons. Finally, we presented the schematic and layout of noise implementation into gating variables that is essentially based on noise generator.

The main part of this thesis is the study and understanding of the noise generator which allows extending their library of analog operators for computing the Hodgkin-Huxley

formalism to a library of stochastic analog operators. In detail, we propose the proof of the solution of SDE (in section 2.3) in continuous time, necessary to obtain the stochastic model. We also detail the hardware implementation of the noise generator. Finally the stochastic behaviours observed in biological neurons have been reproduced in hardware simulations realistically.

6.1 Future work

The noise generator, HN, IN and CPR neurons will be included in the Hysnet chip that will send to manufacturer in autumn 2012. After the chip manufacturation, our research team should create a dedicated PCI, for interfacing the IC to the computer. This PCI board is controlled by an FPGA that allows the sending of command parameters to the IC. It will be realized with the same method of construction used to make that of the previous work of the group. The calibration phase will be done in collaboration with our Taiwanese colleagues. After having calibrated the ASIC, it will be connected to the biological neural network thanks to National Tsing Hua University setup. The interaction between the biological network and the hardware network will probably allow biologists understand better the operation of the noise in a neural network.

Bibliography

[1] Wulfram, G., and Werner, M. K. (2002). Spiking Neuron Models: Single Neurons, Populations, Plasticity. Cambridge University Press.

[2] Structure of a typical neuron. http://www.appsychology.com/Book/Biological/ neuroscience.htm

[3] Chemical synapse. http://apps.cmsfq.edu.ec/biologyexploringlife/text/chapter28/ concept28.2.html

[4] Grassia, F., Burhry, L., Levi, T., Tomas, J., Destexhe, A. and Saighi, S. (2011). Tunable neuromimetic integrated system for emulating cortical neuron models Neuroscience

[5] Pospischil, M., Toledo-Rodriguez, M., Monier, C., Piwkowska, Z., Bal, T., Fregnac, Y., Markram, H., and Destexhe, A. (2008). Minimal Hodgkin- Huxley type models for differ-ent classes of cortical and thalamic neurons. Biol. Cybern. 99, 427-441.

[6] Chow, C.C. and White, J.A. (1996). Spontaneous action potentials due to channel fluctuations, Biophys. J. 71 3013-3021.

[7] Schneidman , E., Freedman, B. and Segev, I. (1998). Ion channel stochasticity may be critical in determining the reliability and precision of spike timing, Neural Comput. 10 1679-1703.

[8] White, J.A., Rubinstein, J.T. and Kay, A.R. (2000). Channel noise in neurons, TINS 23 131-137.

[9] Fellous, J.M., Rudolph, M., Destexhe, A. and Sejnowski, T. J. (2003). Synaptic background noise controls the input/output characteristics of single cells in an in vitro model of in vivo activity Neuroscience 122 811-829

[10] Faisal, A.A., Selen, L.P.J. and Wolpert D.M. (2008). Noise in the nervous system. Nat Neurosci 9: 292-303.

[11] Rolls, E.T. and Deco, G. (2010). The noisy brain: stochastic dynamics as a principle of brain function. New York: Oxford University Press.

[12] Softky, W. andKoch, C. (1993). The highly irregular firing pattern of cortical cells is inconsistent with temporal integration of random epsps. J . Neurosci., 13:334-350.

[13] Higham, D.J. (2001). An algorithmic introduction to numerical simulation of stochastic differential equations, SIAM Rev. 43 525-546.

[14] Sanz-Solé, M. (2010). An introduction to stochastic calculus. http://www.mat.ub.edu/ sanz/cursos/lecturenotes-sc2008.pdf

[15] Oksendal, B. (2000). Stochastic differential equations. Springer 21-72

[16] Saarinen, A., Linne, M.L. and Yli-Harja, O. (2008). Stochastic differential equation model for cerebellar granule cell excitability. PLoS Compu Biol 4: e1000004. doi:10.1371/journal.pcbi.1000004.

[17] Goldwyn, J.H. and Shea-Brown, E. (2011). The What and Where of Adding Channel Noise to the Hodgkin-Huxley Equations. PLoS Comput Biol 7(11): e1002247. doi:10.1371/journal.pcbi.1002247.

[18] Saarinen, A., Linne, M.L. and Yli-Harja, O. (2006). Modeling single neuron behaviour using stochastic differential equations Neurocomputing 69 1091-1096.

[19] Linaro, D., Storace and M. and Giugliano, M. (2011). Accurate and fast simulation of channel noise in conductance-based model neurons by diffusion approximation. PLoS Comput Biol 7: e1001102. doi:10.1371/journal.pcbi.1001102.

[20] Chen, H.,Saighi, S.,Buhry, L. and Renaud, S. (2010).Real-time simulation of biologically realistic stochastic neurons in VLSI. IEEE Trans. Neural Netw. 21, 1511-1517.

[21] Bahar, S. and Moss, F. (2004).Stochastic resonance and synchronization in the crayfish caudal photoreceptor. Mathematical-Biosciences 188, 81-97.

[22] Chen, C.H. (2011). A Conductance-based Neuronal Network in VLSI for Studying the Neural Circuit of the Crayfish. Master's thesis, National Tsing Hua University

[23] Saighi, S., Bornat, Y., Tomas, J., Le Masson , G. and Renaud, S. (2011). A library of analog operators based on the Hodgkin-Huxley formalism for the design of tunable, real-time , silicon neurons. IEEE Trans.Biomed. Circuits Syst. 5, 3-19.

[24] Cauwenberghs, G. (1999). Delta-Sigma Cellular Automata for Analog VLSI Random Vector Generation. IEEE Trans. Circuits Syst.-II: VOL. 46, NO. 3.

[25] Chou, W., and Gray, R. M. (1992). Modulo sigma-delta modulation. IEEE Trans. Commun., vol. 40, pp. 1388-1395.

[26] Nys, O. J. A. P., and Dijkstra, E. (1993). On configurable oversampled A/D converters. IEEE J. Solid-State Circuits, vol. 28, pp. 736-742.

[27] Uchimura, K., Hayashi, T., Kimura, T., and Iwata, A. (1988). Oversampled A- to-D and D-to-A converters with multistage noise shaping modulators. IEEE Trans. Acoust., Speech, Signal Processing, vol. ASSP-36, pp. 1899-1905.